Augmentation of Jet Impingement Heat Transfer on a Grooved Surface Under Wet and Dry Conditions

Abdulmohsen Omar Alsaiari

Dissertation submitted to the faculty of the Virginia Polytechnic Institute and State University in partial fulfillment of the requirements for the degree of

Doctor of Philosophy

In

Mechanical Engineering

Thomas E. Diller - Chair

Jonathan B. Boreyko

Rui Qiao

Scott T. Huxtable

Yang Liu

11/06/2018

Blacksburg, VA

Keywords: Array Jet Impingement Cooling, Power Plant, Air-Cooled Condensers, Entrainment Effect, Jet Impingement Model, Discharge Coefficient, Coefficient of Performance, Grooved Surface, Cooling Towers, Hybrid Cooling, Water Consumption

Augmentation of Jet Impingement Heat Transfer on a Grooved Surface Under Wet and Dry Conditions

Abdulmohsen Omar Alsaiari

ABSTRACT

Array jet impingement cooling experiments were performed on flat and grooved surfaces with the surface at a constant temperature. For the flat surface, power and temperature measurements were performed to obtain convection coefficients under a wide range of operating conditions such as jet speed, orifice to surface stand-of distance, and open area percentage. Cooling performance (*CP*) was calculated as the ratio between heat transfer and fan power. An empirical model was developed to predict jet impingement heat transfer taking into account the entrainment effects. Experimental results showed that jet impingement can provide high transfer rates with lower rates of cooling cost in comparison to contemporary conventional techniques in the industry. *CP* values over 279 were measured which are significantly higher than the standard values of 70 to 95 in current technology. The model enhanced prediction accuracy by taking into account the entrainment effects; an effect that is rarely considered in the literature. Experiments on the grooved surfaces were performed at dry and wet surface conditions. Under dry conditions, results showed 10%~55% improvement in heat transfer when compared to the flat surface. Improvement percentage tends to be higher at wider gaps between the array of orifices and the grooved surface. An improvement of 30%~40% was observed when increasing Re either by increasing orifice diameter or jet speed. Similar improvement was observed at higher flow open area percentages. No significant improvement in heat transfer resulted from decreasing the size of the grooves from 3.56mm to 2.54mm. Similarly, no noticeable change in heat transfer resulted from changing the relative position of the jets striking the surface at the top of the grooves to the bottom of the grooves. Deeper grooves with twice the depth gave statistically similar average heat

transfer coefficients as shallower grooves. Under wet conditions, a hybrid cooling technique approach was proposed by using air jets impinging on a grooved surface with the grooves containing water. The approached is proposed and evaluated experimentally for its feasibility as an alternative for cooling towers of thermoelectric power plants. Convection heat and mass transfer coefficients were measured experimentally using the heat mass transfer analogy. Results showed that hybrid jet impingement provided high magnitudes of heat flux at low jet speeds and flow rates. High coefficients of performance CP > 3000, and heat fluxes > 8,000W/m^2 were observed. Hybrid jet impingement showed 500% improvement as compared to jet impingement on a dry flat surface. CP values of hybrid jet impingement is 600% to 1,500% more as compared to performance of air-cooled condensers and wet cooling towers. Water use for hybrid jet impingement cooling is efficient since evaporation energy is absorbed from the surface directly instead of cooling air to near wet-bulb temperature

Augmentation of Jet Impingement Heat Transfer on a Grooved Surface Under Wet and Dry Conditions

Abdulmohsen Omar Alsaiari

GENERAL AUDIENCE ABSTRACT

This thesis explored the possibility of using air jets on the outside surface of a device that is used to condense steam. An experiment apparatus was used to imitate the conditions of steam condensation in the lab. A flat metallic surface was heated by placing an electric heater beneath it. The metallic surface was cooled using air jets coming out of orifices situated above the hot metallic surface. A fan, connected to an electric motor, was used to create the air jets. The amount of heat transfer was measured by measuring the electric power the heater consumed. This measured power was compared to the power needed to run the fan. The ratio of heat transfer to fan power is called the coefficient of performance CP. The CP values of more than 200 were obtained when air jets were used meaning that we need one kilowatt of mechanical power to remove 200 kilowatts of heat. This CP value is 300% more than the current technology used in the industry where CP ranges from 70 to 90. This means that we can build very efficient steam condensers for power plants. This type of condensers that uses air jets allows the power plant to be efficient and to be able to increase the amount of power generated without extra cost.

Further enhancement of the CP can be achieved by making the hot surface grooved instead of flat with the grooves containing water. Air jets, coming out of orifices situated above the grooved surface, were used for cooling. The CP values of more than 3,000 were obtained when air jets were used with wet grooved surface. This CP values is 1,500% more than the current technology used in the industry. This type of condensers that uses air jets on wet grooves allows the power plant to be efficient and to be able to tremendously increase the amount of power generated without extra power and water costs.

DEDICATION

I would like to dedicate this thesis to my father Omar Mohsen Alsaiari and my mother Latifah Hussein Sultan for their love, compassion, support and guidance they unconditionally provided over the course of my study and my life. I would like also to dedicate this thesis to the love my life, my wife, Nouf M. Binthabit for she is always has been a constant source of happiness, joy, and support. I would extend the delectation to my kids Salman and Omar; the most precious of all.

ACKNOWLEDGEMENTS

I would like to acknowledge professor Thomas E. Diller and my committee members for their advice and guidance which both were essential to completing this thesis. I also would like to acknowledge my lab mates Abdulrahman Alghamdi and Holly Leonard for their help in data collection and processing. I would like to acknowledge King Abdulaziz University for providing the financial support that was imperative for my studies at Virginia Tech.

Table of Contents

List of Figures

List of Tables

Paper 1: The Feasibility of Employing Jet Impingement Cooling in the Condensers of Thermoelectric Power Plants – Experimental Study

Abdulmohsen O. Alsaiaria,b

Department of Mechanical Engineering, Virginia Tech, Goodwin Hall, 635 Prices Fork Road, Blacksburg, VA- 24061

aoa212@vt.edu,

Thomas E. Diller,

Department of Mechanical Engineering, Virginia Tech, Goodwin Hall, 635 Prices Fork Road, Blacksburg, VA- 24061; tdiller@vt.edu

Abstract

This paper presents the findings of an experimental study to evaluate air jets for the use in the condensers of thermoelectric power plants. A constant temperature heated plate was subjected to vertical jets of air pressurized out of orifices. Power and temperature measurements were performed to obtain convection coefficients. Cooling performance (*CP*) was calculated as the ratio between heat transfer and fan power. Tests were performed over a wide range of operation parameters. Also, an empirical model was developed to predict jet impingement heat transfer taking into account the entrainment effects. Experimental results showed that jet impingement can provide high transfer rates with lower rates of cooling cost in comparison to contemporary conventional techniques in the industry. *CP* values over 279 were measured which are significantly higher than the standard values of 70 to 95 in current technology. The aforementioned model enhanced prediction accuracy by taking into account the entrainment effects; an effect that is rarely considered in the literature.

1.1 Introduction

Rising ambient temperatures caused incidents of shutdowns at power plants in the summers of 2011 and 2012 [1]. Because of the associated condenser limitations, it is important to be able to enhance the effectiveness of the condenser in a steam Rankine power cycle. In the design stage, it is desired to condense steam at lower temperatures to decrease the turbine back pressure and enhance the power output. Consequently, it is important to maximize the heat transfer between the surface of the condenser and the cooling medium. A 500 MW power plant operating at 42% thermal efficiency requires the transfer of 700 MW of thermal power to the environment. New environmental regulations prohibit new plants from dumping this thermal energy into water reservoirs. The remaining option is to use ambient air for cooling. Air can be used solely for cooling as in A-frame air-cooled condensers (ACCs) or it can be used with water evaporation such as in cooling towers. ACCs provide large surface area for heat transfer but correspond to relatively low heat transfer coefficients. Moreover, performance is limited by maldistribution of the air flow through the tube bundles [2], fin efficiency, and non-symmetric temperature fields. Cooling towers provide larger capacities for heat rejection; however, they use large quantities of water to make-up for evaporation and requires regular water recycling to limit the build-up of impurities. Moreover, cooling potential is wasted because the air leaves at the wet bulb temperature though it can be utilized in further cooling of steam.

As an alternative, air jet impingement can be used for heat rejection and provides high convective coefficients. The thin boundary layer in stagnation region a jet creates results in higher heat transfer coefficient at lower flow rates and fan power. Extensive studies have examined jet impingement heat transfer since the 1950s. Numerous correlations have been developed since then in an effort to develop generic models for the predictions of heat transfer. However, it has been

proved to be a challenging task to do due to the complex physical nature of the jet impingement problem. One widely known comprehensive study on jet impingement was conducted by Martin [3]. He reported that arrays of jets yielded lower rates of heat transfer than comparable single jets with the same flow rate. Successive studies [4–6] discussed explanations including crossflow of the spent air, interaction between adjacent jets, and entrainment effects of the spent air. Hollworth et al [7] reported that widely spaced jets have smaller interaction effects. Furthermore, crossflow effects can be mitigated by designing the array width to keep the crossflow velocity to be a small fraction of the jet velocity. Entrainment occurs when the jet entrains large amounts of surrounding air in both regions of the free jet and the wall jet. This was attributed to the turbulence generated at the free-shear layers. If entrained air is at a different temperature than the jet, it will change the effective temperature of the jet at the stagnation. This was observed for individual jets and shown to affect the resulting heat transfer [8–11]. It was reported [12] that the integrated heat transfer coefficients match when the temperature of entrainment is matched between single jets and arrays without crossflow.

The current study represents a first step in a paradigm shift from conventional practice for cooling tower or air-cooled heat exchangers. It proposes the use of a novel approach based on jet-impingement of the air onto a flat surface condenser. To minimize the fan power, the air flow rate is purposely kept low, resulting in high exhaust temperatures. One focus of this study is to evaluate the entrainment effect of this exhaust flow on the heat transfer. Entrainment is a key aspect and has been rarely considered in previous studies of jet impingement heat transfer. One reason is the common use of large air flow rates in the relevant studies which means the insignificance of the difference between the inlet and exhaust temperatures. Similarly, fan power has not been considered important for jet impingement heat transfer. However, fan power is a key parameter in

determining the cost of handling the heat load of the condenser in a thermoelectric power plant. Therefore, a second focus of this study is to compare the rates of heat transfer resulting from jet impingement to the fan power. Accordingly, the cooling performance (*CP*) ratio, between the heat transfer and the required fan power, is introduced as an important design parameter. Jet impingement systems are compared with common types of condensers that are currently used in the industry such as ACC's and wet cooling towers.

1.2 Model

An empirical model was developed to predict the average convection heat transfer coefficient, under steady state conditions, resulting from jet impingement on a constant temperature surface. The novel aspect of this model that it specifically includes the effect of air entrainment. The chief assumption of the model is that an array of jets behaves in the same manner as a single jet [13] if the effect of the exhaust flow is included.

1.2.1 Single Jet

A jet is formed when fluid is accelerated through an opening by a pressure difference into the surrounding fluid. This occurs with negligible friction losses, as described by the Bernoulli's equation for low velocities,

$$U_o = \sqrt{\frac{2\Delta p}{\rho}} \tag{1}$$

As the free jet nears the plate surface the velocity decreases to zero at the stagnation point and the static pressure increases. The jet then accelerates as it turns and forms a wall jet [9], as illustrated in figure 1.1. Studies [12,14] showed that for the region of one or two nozzle diameters above the surface of stagnation, the jet flow issuing from the nozzle is not effected by the plate impingement. This means that the free jet region can be studied independently from the impingement plate [14].

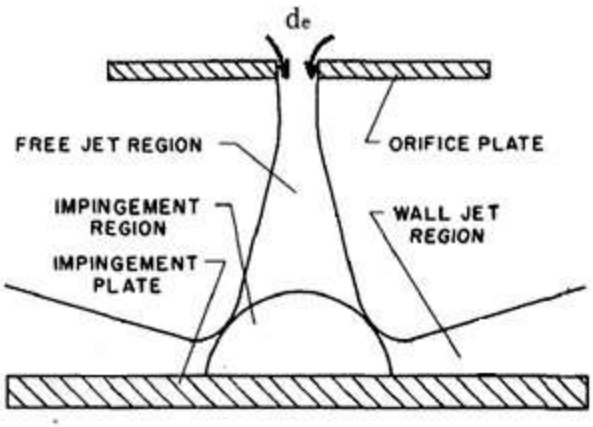

Figure 1. 1: *Fluid flow regions of an impinging jet [9]*

The free jet has an initial potential core region where the centerline velocity remains constant with low turbulence levels [14,15] over the first 6.5 jet diameters [16–18]. A similar thermal core region for the temperature of the jet was observed [19] to extend for 4.5 diameters. Along the length of the thermal core, the centerline temperature remains constant. Beyond both core regions, the centerline velocity and temperature are influenced by the conditions of the entrained surrounding air.

Donaldson et al [20] developed a correlation for heat transfer at the stagnation region of the following form:

$$Nu_{St} = \frac{5.4\sqrt{Re_{d_e}}}{H/d_e} \tag{2}$$

where

$$Nu_{St} = h_{St}(\frac{d_e}{k}) \tag{3}$$

The H/d_e term in the denominator accounts for the decay of the jet centerline velocity due to entrainment of surrounding air. Because the decay only starts after a distance of 6.5 diameters, the denominator has a value of 6.5 for $H/d_e < 6.5$. In the wall jet region, an empirical correlation was adapted from [21], for heat transfer in the wall region as a function of the distance from the stagnation point:

$$Nu_{wj}(r) = \frac{0.0524 \cdot Re_{d_e}{}^{0.8}}{\left(\frac{r}{d_e}\right)^{0.8}} \qquad \text{for} \quad r_{St} \le r \le R \tag{4}$$

where

$$Nu_{wj}(r) = \frac{h_{wj}(r)\, d_e}{k} \tag{5}$$

This is valid for the region outside of the impingement region ($r > r_{st}$). These correlations were developed for the usual academic case of the environment temperature the same as the jet exit temperature.

1.2.2 Multiple Jets and Entrainment

One of the major differences between single jets and jet arrays is the requirement to exhaust the spent air from the space between the jet entrance and the surface as illustrated in figure. 1.2. Because of the large amount of entrainment at the free shear layers, recirculation regions develop which feed exhaust air into the jets. The exhaust air by necessity has already interacted with the surface and consequently is at a higher temperature.

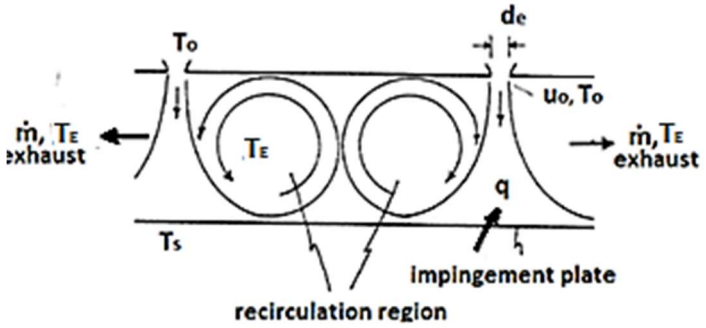

Figure 1. 2: *Array jet flow and circulation.*

A simple energy balance requires that

$$\dot{m}C_p(T_E - T_o) = h_{av}(\pi R^2)(T_s - T_o) \tag{6}$$

The change in enthalpy of the air is balanced by the heat transfer from the surface. The larger the value of the average surface heat transfer coefficient, h_{av}, relative to the mass flow rate, the larger the increase in exhaust temperature. Therefore, an efficient use of the cooling air means that the

exhaust temperature rises higher and its effect on the surface heat transfer must be included. Most reported studies of jet impingement heat transfer have been more concerned with maximizing the heat transfer coefficient instead of the efficiency of using the air and have ignored the effects of entrainment of the exhaust air.

A non-dimensional exhaust temperature can be defined as:

$$F = \left(\frac{T_E - T_o}{T_s - T_o}\right) \tag{7}$$

where the normal values are bounded as $0 \leq F \leq 1$ as shown in equation 7. The temperature decay of the free jet is given by:

$$\frac{T - T_E}{T_o - T_s} = \frac{4.5}{H/d_e} \tag{8}$$

for $H/d_e > 4.5$ [19]. The heat flux at the stagnation point is proportional to the actual temperature difference of the jet relative to the surface temperature, $T - T_s$. Therefore, the degradation of the heat flux due to the entrainment of exhaust is equal to the ratio of the temperature differences and is given the symbol G_{St}.

$$G_{St} = \frac{T - T_s}{T_o - T_s} = \left(\frac{4.5}{H/d_e} - 1\right)F + 1 \tag{9}$$

Adding this factor to equation 2 gives heat transfer coefficient relative to the temperature difference from the jet exit, To –Ts.

$$Nu_{St} = \frac{5.4\sqrt{Re_{d_e}}}{H/d_e} G_{St} \tag{10}$$

The effect of entrained air extends, also, to the wall jet region. A correlation for the change of the wall jet temperature in the radial direction due to entrained air at temperature T_E was developed in [22,23] and it takes the form:

$$\frac{T-T_E}{T_o-T_E} = \frac{1.2}{\left(\frac{r}{d_e}\right)^{1.1}} \quad \text{for the wall jet region} \quad r_{St} \le r \le R \tag{11}$$

The corresponding degradation of the surface heat transfer relative to the jet exit temperature is defined in the same way as for the stagnation region:

$$G_{wj} = \frac{T-T_s}{T_o-T_s} = \frac{1.2}{\left(r/d_e\right)^{1.1}} F + (1-F) \qquad \text{for} \quad r_{St} \le r \le R \tag{12}$$

Adding this factor to equation 4 modifies it to include the entrainment effect for a heat transfer coefficient based on the $T_o - T_s$ temperature difference.

$$Nu_{wj} = \frac{0.0524\, Re_{d_e}^{0.8}}{\left(r/d_e\right)^{0.8}} G_{wj} \qquad \text{for} \quad r_{St} \le r \le R \tag{13}$$

The latter equation is applicable for r values beyond the stagnation region for $r > r_{St}$ where r_{St} is the radius of the stagnation region. Because of the spread of the jet with distance from the orifice, the size of the stagnation region increases with jet height. For $H/d_e \ge 6.5$ the ratio $\left(\frac{r_{St}}{d_e}\right) = 0.27 H/d_e$, while in the core region ($H/d_e < 6.5$) the value of $\left(\frac{r_{St}}{d_e}\right) = 1.75$.

To test the validity of the heat transfer correlations, a series of experiments were performed with a single jet under controlled entrainment air temperatures. A 3-mm diameter Gardon heat flux gage by Medtherm was mounted flush in the heated aluminum plate with control of the surrounding air temperature as described in [8]. Because the gage used had low sensitivity, the temperature differences developed across the gage were limited and the resulting corrections for convection measurements were small as described by Borrell and Diller [24]. A low sensitivity Gardon heat flux gage was mounted in the heated aluminum plate. An example of the results is shown in figure 1.3 for two different values of F, the non-dimensional entrainment temperature. The entrainment effect shown by the measured data points is clearly captured by the analytical lines representing equation 13 in the wall jet region. In the stagnation region there is very little

effect of entrainment because of the small height. Most of the jet is in the core temperature region of 4.5 diameters.

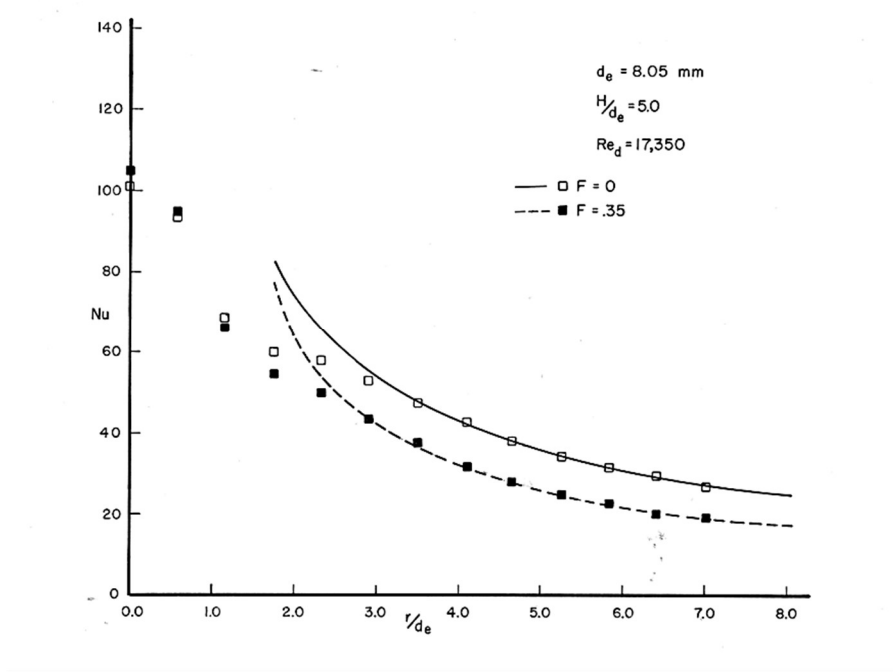

Figure 1. 3: *Entrainment effect in the wall jet region, experiments are data points, wall jet correlations are lines.*

1.2.3 Average Heat Transfer Coefficients

The analysis done on the stagnation and wall jet regions resulted in modified correlations that take into account the effect of entrainment on heat transfer. It is assumed that heat transfer has a linear relation in the stagnation region, $r = 0$ *to* $r = r_{St}$. Therefore, integrating equations 10 (from $r = 0$ to $r = r_{St}$) and 13 (from $r = r_{St}$ to $r = R$), for a surface area, gives the following expression for the average Nusselt number.

$$Nu_{av} = \frac{0.0524\,Re^{0.8}}{\left({}^{R}/_{d_e}\right)^2}\left\{\frac{\left({}^{r_{St}}/_{d_e}\right)^2}{3}\left[\frac{Nu_S}{0.0524\,Re_{d_e}{}^{0.8}} + \frac{2}{\left({}^{r_{St}}/_{d_e}\right)^{0.8}}\left(\frac{1.2}{\left({}^{r_{St}}/_{d_e}\right)^{1.1}}F + (1-F)\right)\right] + \right.$$

$$\left. 24\left[\left({}^{R}/_{d_e}\right)^{0.1} - \left({}^{r_{St}}/_{d_e}\right)^{0.1}\right]F + \frac{5}{3}\left[\left({}^{R}/_{d_e}\right)^{1.2} - \left({}^{r_{St}}/_{d_e}\right)^{1.2}\right](1-F)\right\} \qquad (14)$$

Where:

$$Nu_{av} = \frac{h_{av}\, d_e}{k} \tag{15}$$

The value of R in equation 14 represents the average radius of the area served by an individual jet. For an array of jets, this radius and the total surface area are related as:

$$R = \sqrt{A_s/(N\pi)} \tag{16}$$

The open area is a convenient non-dimensional ratio of jets total correctional area to the total surface area of impingement:

$$A_o = \left(N\frac{\pi}{4}{d_e}^2\right)/(\pi R^2) = \left(\frac{d_e}{2\,R}\right)^2 \tag{17}$$

The model assumes that the entrained air temperature T_E to be the exhaust temperature. The value of T_E is dictated by the energy balance in equation 6. Inserting $\dot{m} = (A_o A_s)\rho U_o$ and non-dimensionalizing the equation results in a relation between F and Nu_{av}

$$F = \frac{Nu_{av}}{Re_{d_e} Pr_{\ o}} \tag{18}$$

A major focus of the current study is to evaluate jet impingement for the application in thermal power plants condensers as an alternative to ACCs and wet cooling towers. Evaluation can be done by comparing the heat transfer in each technique resulting from the same fan power. For that purpose, the cooling performance CP is introduced and is defined as the ratio between the heat transfer from the surface and the fan power. The following is the definition of CP:

$$CP = \frac{Q}{P_f} \tag{19}$$

The heat transfer, for $T_s > T_o$, and the fan power are, respectively, calculated as:

$$Q = A_s \cdot h_{av} \cdot (T_s - T_o) \tag{20}$$

$$P_f = \frac{\dot{\forall} \cdot \Delta p}{\eta_f} \tag{21}$$

Where η_f is the fan efficiency and was assigned a value of 65% and $\dot{\forall}$ is the volume flow rate. Therefore, for the jet impingement system:

$$CP = h_{av} \cdot (T_s - T_o) \cdot \frac{2 \cdot \eta_f}{(A_o) \cdot \rho \cdot {U_o}^3} \quad (22)$$

In summary, the current model used a semi-empirical approach to quantify and include the effect of the entrained air on jet impingement heat transfer. This was applied to the average heat transfer for arrays of jets. The results are then compared with extensive experimental testing.

1.3 Experimental Setup

1.3.1 Design and Fabrication of Jet Arrays

Six different jet plates were made by drilling holes in 1.6 mm (1/16") aluminum plates. As shown in figure 1.4, three of the plates have the same value of the open area A_o =1.5% but at different orifice diameters of 3.18mm, 4.76mm, and 6.35mm. The diameter of orifices in the remaining plates was fixed at 4.76mm while the value of A_o was varied with values of 1%, 1.5%, 2%, and 3%. The number of orifices and the configuration in each plate is given by:

$$N = \frac{A_o \cdot A_s}{C_D \cdot \frac{\pi}{4} \cdot {d_e}^2} \quad (23)$$

The plates were fabricated in a CNC mill to ensure that all orifices in each plate have the same geometrical characteristics.

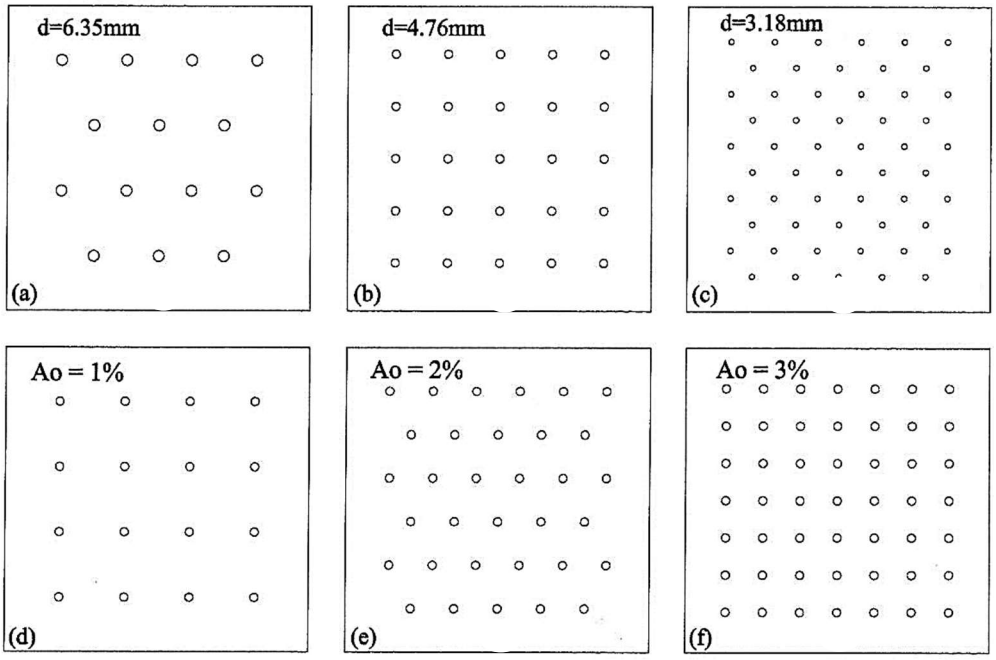

Figure 1. 4: *Orifices plates: upper row A_o=1.5%, lower row d=4.76mm.*

Most jet arrays are produced using orifices in thin plates with discharge coefficients of C_D = 0.75 to 0.85, because of the contraction of the flow as it turns through the orifice. This gives an effective diameter of:

$$d_e = d\sqrt{C_D} \tag{24}$$

Although shown to be important to the resulting heat transfer [25], many jet array studies overlook this effect. To measure C_D, a random sample of orifices were selected in each orifices plate. Reynolds number based on the orifice diameter for different air speeds were matched for water to obtain the respective water jet speeds $U_{o,w}$. A water head pressure was maintained at a prescribed level by regulating water flow to the container with the orifice plate beneath it. Water was allowed to flow through only the selected orifice and the flow rate of water $\dot{m}_w$ was measured using an electronic weight scale and a timer. The discharge coefficient then was calculated as:

$$C_D = \frac{\dot{m}_w}{\rho_w \cdot \frac{\pi}{4} \cdot d^2 \cdot {U_{o,w}}^2} \tag{25}$$

Table 1 shows the measured discharge coefficients for the three different orifice sizes.

Table 1. 1: *Discharge coefficients, CD*

d(mm)	n	C_D	Standard deviation	d_e(mm)
3.18	6	0.784	0.003	2.81
4.76	6	0.785	0.005	4.22
6.35	6	0.802	0.002	5.69

1.3.2 Apparatus

The experimental apparatus for measuring the average surface heat transfer is depicted in figure 1.5. A wind tunnel was used to supply air for the experiment at varying jet speeds by regulating the power supplied to an axial flow fan. A manometer was used to measure the static pressure in a vicinity of the orifice opening inside the plenum, though not shown in the figure. Appropriate Δp was maintained to satisfy the required jet speed as described by equation 1. A pitot tube was used to measure the jet velocity for a random sample of jets at each orifices plate to insure uniform exist velocity.

Unlike the actual application for condensation, the surface was heated electrically and the air was cooler. This provided an easier system for measuring the heat transfer coefficient between the jets and the surface. The aluminum test plate has a thickness of 12.7 mm and is heated using an electric heater placed beneath it. A total of 14 T-type thermocouples were distributed and press fit into the plate flush with the surface. Eight thermocouples were wired in parallel and supplied to a Eurotherm 810 PID temperature controller. The controller was used with a Eurotherm 831 Silicon Control Rectifier (SCR) to supply power to the heater. Therefore, it is necessary to use a true-RMS voltmeter (HP-3486A) to measure the voltage to determine the power supplied to the heater. Temperature readings from the remaining six thermocouples were recorded using an NI-9214 DAQ system.

To minimize edge losses, four guard plates surrounded the test plate and were maintained at the same set-point temperature of the test plate using similar PID controllers. The test plate and the

guard plates were placed on a multilayer of insulation materials of wood and fiberglass to minimize the conduction losses.

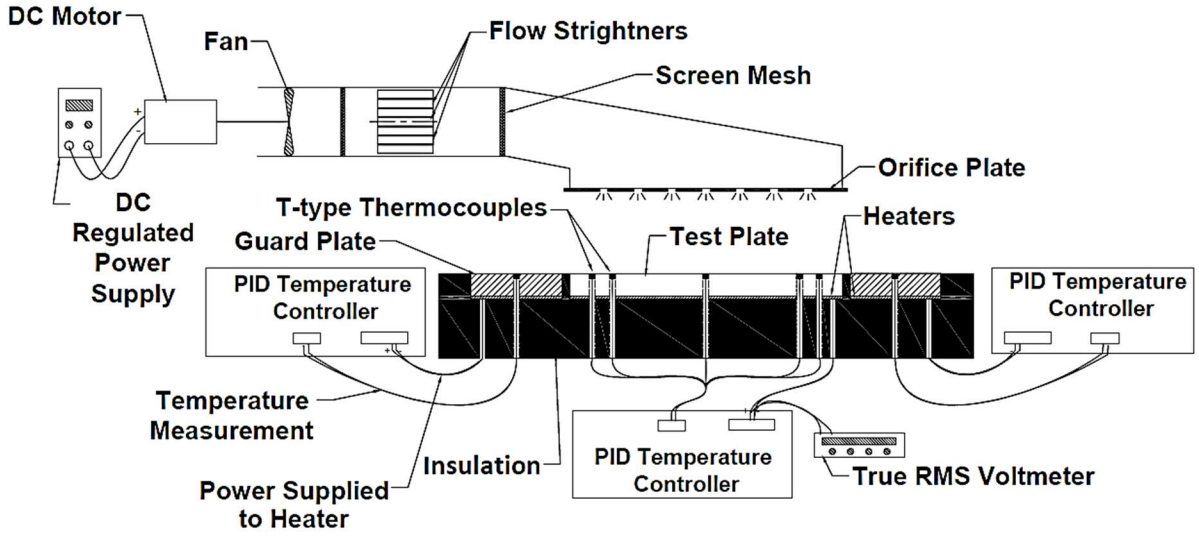

Figure 1. 5: *Abstract depiction of the experiment apparatus*.

1.4 Data Analysis

1.4.1 Procedure

Average heat transfer coefficients were obtained through the measurement of power supplied to the heater that was required to sustain the surface temperature T_s of the test plate. The system typically requires 25 minutes to reach steady state at which, T_s, T_o, and V are recorded. Surface temperature T_s was obtained by averaging temperature readings of six thermocouples uniformly distributed on the test surface. A standard deviation of 0.3°C was observed on T_s readings across the plate spatially. Accordingly, the surface temperature can be treated as constant. The ambient temperature T_o was logged using a thermocouple placed inside the wind tunnel. The electrical power density $\mathcal{P}/A_s$ supplied to the heater at steady state was calculated as:

$$\frac{\mathcal{P}}{A_s} = \frac{V^2}{\mathcal{R}A_s} \tag{26}$$

Accounting for the conduction and radiation losses, the convection heat flux from the surface is isolated as:

$$q^{"}_{conv} = \frac{\mathcal{P}}{A_s} - q^{"}_{cond} - q^{"}_{rad} \quad (27)$$

And the average convection heat transfer coefficient is obtained as:

$$h_{av} = \frac{q^{"}_{conv}}{T_s - T_o} \quad (28)$$

1.4.2 Heat Losses

The conduction heat losses q"$_{cond}$ were divided into lateral loss and downward loss. The lateral loss was significantly diminished due to the use of four guard plates surrounding the test plate and the loss was neglected. The downward loss was estimated as 1% of the power dissipated by the heater. This estimation was obtained through thermal resistances analysis for the upward and downward mediums enclosing the heater. The radiation loss was calculated, assuming the surrounding is at the initial jet temperature, as:

$$q^{"}_{rad} = \varepsilon\sigma(T_s^4 - T_o^4) \quad (29)$$

The surface emissivity ε value was found to be 0.76. This estimation was obtained by using FLIR SC600 Series High-Resolution LWIR Science-Grade infrared camera where a portion of the test plate was painted with a black paint with a known value of ε_b= 0.94, while another portion remained unpainted. The plate was maintained at a known temperature value using the PID controller. An infrared picture of the plate was captured and indicated different temperatures for the painted and unpainted portions of the plate. Accordingly, the emissivity of the plate was obtained as:

$$\varepsilon = \frac{T^4_{unpainted}}{T^4_b} \cdot \varepsilon_b \quad (30)$$

Accordingly, the percentage of heat transfer due to radiation was found to vary from 2.5% to 10% of $\mathcal{P}$. The extremes of this interval were determined by the surface temperature and the value of the convection coefficient. For example, the 2.5% was observed at high value of convection coefficient and T_s= 42.8ºC.

1.4.3 Data Statistics and Uncertainty

Confidence intervals were constructed for the measured values of Nu_{av}. For each test, 36 measurements of Nu_{av} were recorded giving the mean value, standard deviation, and the 95% confidence interval. It was observed that the size of the confidence interval varied between 2% to 3% of the estimated mean value of Nu_{av}.

The sources of uncertainty in the measurement of Nu_{av} are listed on table. 2 with the respective uncertainty values. Parameters were selected based on the expression that was adopted to calculate Nu_{av} through the measurement of Voltage V, electrical resistance $\mathcal{R}$, and temperature T. The average Nusselt number Nu_{av} was obtained as:

$$Nu_{av} = \frac{h_{av}\, d_e}{k} = \frac{V^2/\mathcal{R}}{(T_S - T_o)A_S} \cdot \frac{d_e}{k} \tag{31}$$

Therefore, the uncertainty on Nu_{av} was estimated as

$$U_{n_{(Nu_{av})}} = \left\{\left[\frac{\partial}{\partial V}(Nu_{av}) \cdot U_{n_V}\right]^2 + \left[\frac{\partial}{\partial \mathcal{R}}(Nu_{av}) \cdot U_{n_{\mathcal{R}}}\right]^2 + \left[\frac{\partial}{\partial d_e}(Nu_{av}) \cdot U_{n_{d_e}}\right]^2 + \left[\frac{\partial}{\partial T}(Nu_{av}) \cdot U_{n_T}\right]^2 + \left[\frac{\partial}{\partial A_s}(Nu_{av}) \cdot U_{n_{A_s}}\right]^2 + \left[\frac{\partial}{\partial k}(Nu_{av}) \cdot U_{n_k}\right]^2\right\}^{\frac{1}{2}} \tag{32}$$

The resulting value of estimated uncertainty Nu_{av} was 4%.

Table 1. 2: *Sources of uncertainty for the flat surface.*

#	Source of uncertainty	Value	Unit
1	Voltage measurement, U_{n_V}	0.02% of measured V	volt
2	Resistance measurement, $U_{n_{\mathcal{R}}}$	0.5% of of measured $\mathcal{R}$	ohm
3	Temperature measurement, U_{n_T}	0.3	K
4	Surface area measurement, $U_{n_{A_s}}$	3.4×10^{-4}	m^2
5	Thermal conductivity value, U_{n_k}	1.3×10^{-4}	W/(m-K)
6	Orifice diameter measurement, $U_{n_{d_e}}$	4×10^{-5}	m

The 3% confidence interval value of the data and the 4% estimated uncertainty of the Nu_{av} are both indicators of the good quality of the experiment and of the results produced.

1.5 Results and Discussion

To investigate the effect of surface temperature on the heat transfer coefficient, a majority of the experiments were performed with two different surface temperatures, T_s= 42.8ºC and 60ºC. The results in figure 1.6 show that statistically the convection coefficient is the same for both temperatures, as expected. Therefore, the remaining results are only presented for T_s= 42.8ºC. The solid and dashed curves represent results obtained using the current model. The figure, shows a decrease of Nu_{av} as H/d_e increased and the uncertainty of the experiment measurement is represented by bars on each measurement. One can notice an increase in heat transfer by 90% as the A_o increases from 1% to 3% at all H/d_e ratios. Increasing the flow rate by a factor of three, by tripling A_o, only resulted in increasing the heat transfer only by a factor of two. Furthermore, when H/d_e decreased from 12 to 3.6, the heat transfer increased by 40% at A_o =3%, and 23% at A_o =1%, respectively. The latter suggests that heat transfer is more receptive to changes in H/d_e ratio at higher A_o percentages.

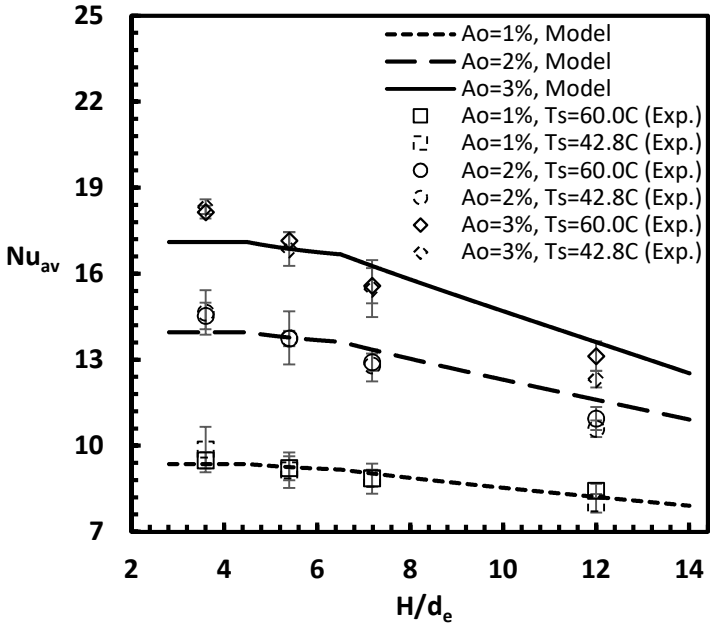

Figure 1. 6: *Variation of Nu_{av} vs H/de for Re_{de}=2,660 at T_s=42.8°C and T_s=60°C.*

The variation of F with H/d_e is shown in figure 1.7 for cases of A_o =1.5% and A_o =3% at Re_{de} = 2,660. The solid and dashed curves represent results obtained using the current model. Experimental results of F were obtained by invoking the measured Nu_{av}, Re_{de}, and A_o into equation 18. This is because it is challenging to get a direct measurement of the T_E because of the complex nature and instability of the flow patterns of the entrained air between the jets. The graph shows a reduction in F, and thus in the exhaust temperature, as H/d_e increases because of the lower heat transfer coefficient. Another observation is that F is higher at A_o =1.5% than A_o =3% even though heat transfer is higher at the latter. This means that heat is transferred more efficiently transferred at lower flow rates and H/d_e ratios.

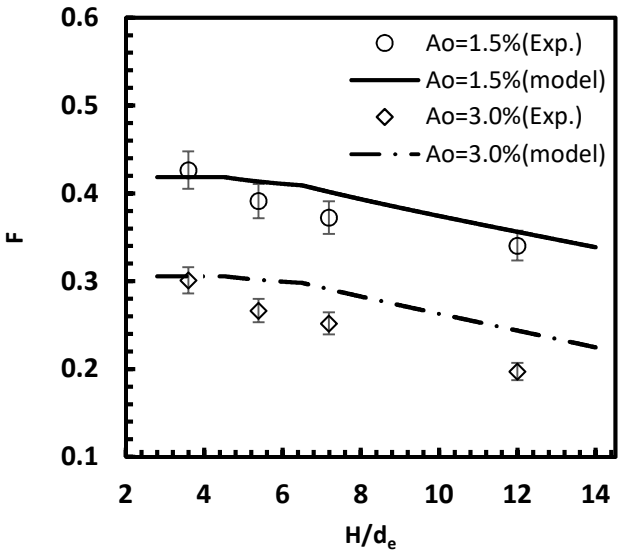

Figure 1. 7: *Entrainment factor F vs H/d_e for Re_{de} =2,660*

The average Nu_{av} variation with Re_{de} is depicted in figure 1.8 for A_o =1.5%. The graph shows an increase in Nu_{av} as Re_{de} increases. It can be noticed that when Re_{de} increased by eight times, the heat transfer increased by a factor of 5.5 at H/d_e=3.6 and 4.4 at H/d_e=12. The variation of corresponding F is shown in figure 1.9 and one can note that for the same Re_{de}, F is higher at the H/de=3.6. Also, F tends to decrease as Re_{de} increases which means that the efficiency of heat transfer, in terms of the exhaust temperature, decreases at higher Re_{de} values.

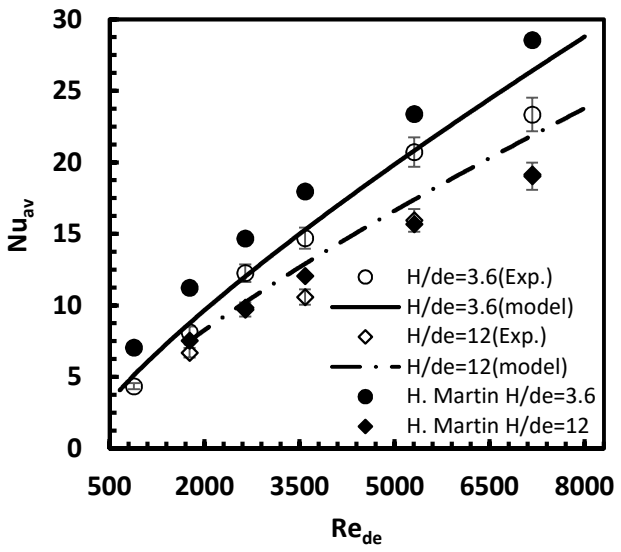

Figure 1. 8: *Nu_{av} vs Re_{de} for A_o=1.5%*

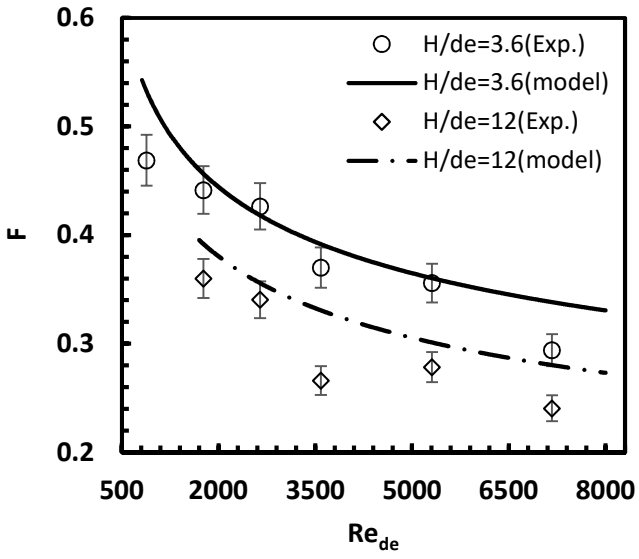

Figure 1. 9: *Entrainment factor F vs Re_{de} for A_o=1.5%*

The model gave accurate predictions for the case of lower H/d_e ratio of 3.6, where entrainment effects are dominant, as compared to results obtained using the correlation in [3], which does not explicitly account for the entrainment effect. Also, accurate predictions were obtained at lower A_o percentages. The accuracy of prediction of the current model decreased as H/d_e and/or A_o increased. One explanation is that the model assumes that an array of jets behaves in the same manner as single jets, an assumption that implies the effects of the interaction between adjacent jets to be insignificant. However, the latter effects increase as the H/d_e ratio increases and/or the A_o percentage increases. The increase of A_o means in an increase of the number of jets for the same orifice diameter as expressed by equation 22. It is expected that under such conditions of high H/d_e ratio and/or A_o percentage that the free jets overlap before and/or at the point of stagnation compromising the momentum and temperature at which the jets strike the surface. This is illustrated in figure 1.10 and 1.11. The model would result in an over prediction, up to 21%, of the heat transfer coefficients under these conditions as shown in figures 1.7 to 1.9 for H/d_e = 12 and A_o=3%.

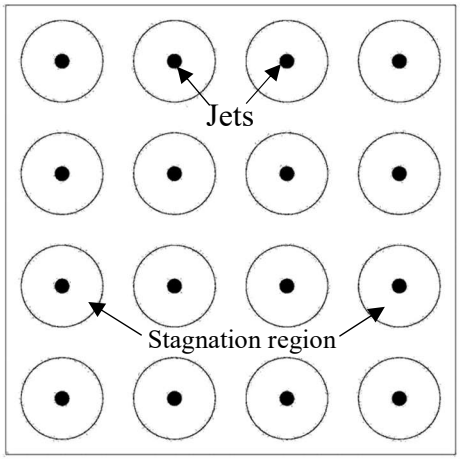

Figure 1. 10: *Approximation of the stagnation area d=4.76mm, A_o=1% and H/d_e=12*

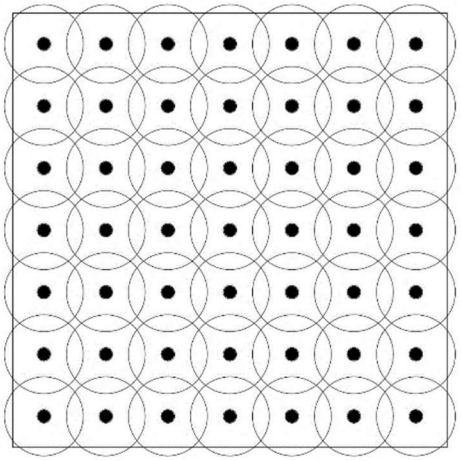

Figure 1. 11: *Approximation of the stagnation area d=4.76mm, A_o=3% and H/d_e=12*

The cooling performance *CP* was calculated as the ratio of the heat transfer and the fan power. A value of 65% fan efficiency was assigned in calculating *CP* using equation 22. In a sense, *CP* pays emphasis on the idea of cost in terms of fan power, verses gain in terms of the corresponding heat transfer. This idea is rarely applied in the context of jet impingement heat transfer. Figure 1.12 shows the variation of *CP* with the open area A_o, and Re_{de} at H/d_e =3.6 for $(T_s - T_o) = 18^oC$. Similar behavior of variation was observed at H/d_e =12 with a minor decrease of 20% in *CP* at the same A_o and Re_{de}. The results illustrate that jet impingement is efficient, especially when conducted at lower jet speeds yielding *CP* ratios of around 600. A direct linear relation was observed between *CP* and $(T_s - T_o)$ at which the test is performed. This translates into doubling *CP* values at the graph for $(T_s - T_o) = 36^oC$ yielding a *CP* ratio of more than a 1000. Figure 1.13 depicts this in a general representation by using $CP/(T_s - T_o)$ as the vertical axis. This graph is particularly helpful for design considerations. For example, at Re=1800 and H/de=3.6 a value of 5 per each ^oC is shown.

Another key observation is that the *CP* drops with a faster rate as the jet speed U_o increases since $CP \propto U_o^{-3}$ as described by equation 22. It was observed that doubling jet speed U_o yielded

an increase of 60% in heat transfer rates, however, *CP* decreased by 80% requiring eight orders of magnitude increase in fan power P_f.

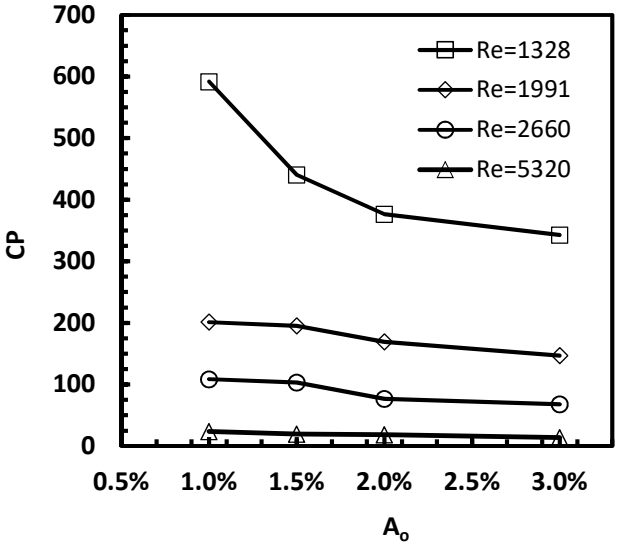

Figure 1. 12 : *CP vs A_o for H/d_e=3.6 and* $\Delta T = 18\ ^oC$

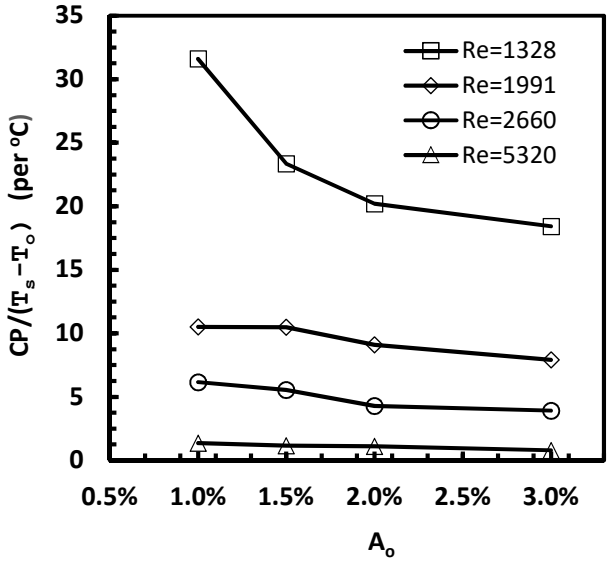

Figure 1. 13: *CP vs Ao for H/d_e=3.6 per °C*

A key aspect the current study is to evaluate if it is advantageous to use air jets in the condensers of thermoelectric power plants. This requires a comparison in performance between the conventional techniques in the industry and the findings of this study. Most of these measured *CP* values are higher than obtained with industry conventional systems such as A-frame air-cooled condensers (ACCs) and cooling towers. According to guidelines established by Electric Power Institute (EPRI) [26] for the required fan power a calculated *CP* ratio of 92 was found to correspond to an ACC operating on $(T_s - T_o) = 27^oC$. Under similar operation conditions for a jet impingement condenser with A_o=1.5%, H/d_e=3.6, the *CP* ratio is 279. The latter ratio represents a 300% improvement in performance that can translate to higher condenser heat rejection capacity and/or lower levels of power required to run the fan. One may argue that the 279 ratio was obtained in a lab environment and comparison with large scale system may not be reprehensive. However, the significant enhancement from 92 to 279 can serve as a strong indicator that jet impingement

carries potential for new efficient condensers systems. A comparison between the *CP* ratios of dry jet impingement and wet cooling towers also shows higher performance in a jet impingement system. Values of *CP* for a commercial tower are provided in [27] in which *CP* of a tower with counter and cross air flow are 36 and 73.5, respectively.

1.5 Conclusion

Jet impingement experiments were conducted in a manner that models a condensation process. The results were used to show that jet impingement is a viable and efficient alternative to A-frame ACC's and wet cooling towers. An efficient heat transfer process results in high exhaust temperatures, which results in a decrease in heat transfer due to entrainment of the exhaust by the jets. This effect was modeled and included in a correlation for jet impingement heat transfer. The correlation yielded good prediction accuracy particularly at conditions where entrainment effects are dominant. The findings of the experiment strongly suggest that jet impingement is an alternative that can provide higher rates of heat transfer at lower fan power requirements. Cooling performance *CP* provides an easy quantification of cost-to-benefit of the system. Much higher *CP* values where demonstrated for jet impingement systems than typical current condensers.

Nomenclature

A	Area (m^2)
Ao	Open area percentage (%)
C_p	Specific heat capacity (J/kg-K)
d	Diameter (m)
h	Convection Coefficient (W/m^2-K), ($h = Nu \cdot k/d$)
H	Orifice to surface distance (m)
k	Thermal conductivity ($W/m\text{-}K$)
$\dot{m}$	Mass flow rate (kg/s)
N	Number of jets
n	Number of experiments
Pf	Electrical power (W)
$\mathcal{P}$	Fan Power (W)
Q	Heat Transfer (W)
q"	Heat flux (W/m^2)

$\mathcal{R}$	Electrical resistance (ohm)
R	Radius of the area served by a jet (m)
r	Radial coordinate from stagnation point (m)
T	Temperature (K)
U	Velocity (m/s)
$U_{n_{A_s}}$	Surface area uncertainty (m2)
$U_{n_{d_e}}$	Orifice diameter uncertainty (m)
U_{n_k}	Thermal conductivity uncertainty (W/m-K)
$U_{n_{\mathcal{R}}}$	Electric resistance uncertainty (ohm)
U_{n_V}	Voltage uncertainty (volt)
V	Voltage (volt)
$\dot{\forall}$	Volume flow rate (m^3/s), ($\dot{\forall} = [A_s \cdot A_o] \cdot U_o$)
XC	Inviscid core length (m)
XT	Thermal core length (m)
Δp	Pressure difference (Pa)
α	Thermal diffusivity (N/m2)
ρ	Density (kg/m^3)
σ	Stefan-Boltzmann Constant ($W \cdot m/K^2$)
υ	Kinematic viscosity (N/m2)

Non-dimensional

CD	Discharge coefficient
CP	Cooling performance
ε	Emissivity
η_f	Fan efficiency, $\eta_f = 0.65$
F	Entrainment factor
G	Degrading factor
Nu	Nusselt number, $Nu = h \cdot d/k$
Pr	Prandtl number, $Pr = \nu/\alpha$
Rede	Reynolds Number based on effective jet diameter, $Re_{d_e} = U_o \cdot d_e/\nu$
$U_{n_{(Nu_{av})}}$	Nusselt number Uncertainty

Subscripts

arbt.	Arbitrary property
av	Average property
b	Black body property
cond	Conduction
conv	Convection
e	Effective property
E	Entrainment property
o	Jet initial property
rad	Radiation

s	Surface Property
St	Stagnation Property
w	Water
wj	Wall jet property

References

[1] J. Rogers, K. Averyt, S. Clemmer, M. Davis, F. Flores-Lopez, P. Frumhoff, D. Kenney, J. Macknick, N. Madden, J. Meldrum, Water-smart power: Strengthening the US electricity system in a warming world, Camb. MA Union Concerned Sci. (2013).

[2] J. Wen, D. Tang, Z. Wang, J. Zhang, Y. Li, F. Sun, Numerical Simulation of Flow and Heat Transfer of a Direct Air-Cooled Condenser Cell in a Power Plant, in: American Society of Mechanical Engineers, 2013: p. V001T03A035-V001T03A035.

[3] H. Martin, Heat and mass transfer between impinging gas jets and solid surfaces, Adv. Heat Transf. 13 (1977) 1–60.

[4] S. Polat, Heat and mass transfer in impingement drying, Dry. Technol. 11 (1993) 1147–1176.

[5] R. Viskanta, Heat transfer to impinging isothermal gas and flame jets, Exp. Therm. Fluid Sci. 6 (1993) 111–134.

[6] K. Jambunathan, E. Lai, M. Moss, B. Button, A review of heat transfer data for single circular jet impingement, Int. J. Heat Fluid Flow. 13 (1992) 106–115.

[7] B. Hollworth, R.D. Berry, Heat transfer from arrays of impinging jets with large jet-to-jet spacing, J. Heat Transf. 100 (1978) 352–357.

[8] S. Striegl, T. Diller, The effect of entrainment temperature on jet impingement heat transfer, J. Heat Transf. 106 (1984) 27–33.

[9] S. Striegl, T. Diller, An analysis of the thermal entrainment effect on jet impingement heat transfer, Am. Soc. Mech. Eng. 1 (1982).

[10] B. Hollworth, L. Gero, Entrainment effects on impingement heat transfer: part II—local heat transfer measurements, J. Heat Transf. 107 (1985) 910–915.

[11] R. Vinze, S. Chandel, M. Limaye, S. Prabhu, Influence of Nozzle Shape and Jet Exit Temperature on Heat Transfer Distribution between a Flat Plate and Impinging Air Jets, (2011).

[12] I. Tani, Y. Komatsu, Impingement of a round jet on a flat surface, in: Appl. Mech., Springer, 1966: pp. 672–676.

[13] M. Gundappa, J. Hudson, T. Diller, Jet impingement heat transfer from jet tubes and orifices, in: 1989: pp. 43–50.

[14] R. Gardon, J.C. Akfirat, The role of turbulence in determining the heat-transfer characteristics of impinging jets, Int. J. Heat Mass Transf. 8 (1965) 1261–1272.

[15] G. Birkhoff, Jets, wakes, and cavities, Elsevier, 2012.

[16] S. Beltaos, N. Rajaratnam, Impinging circular turbulent jets, J. Hydraul. Div. 100 (1974) 1313–1328.

[17] J.W. Gauntner, J. Livingood, P. Hrycak, Survey of literature on flow characteristics of a single turbulent jet impinging on a flat plate, Wash. DC. (1970) 19.

[18] J. Gauntner, P. Hrycak, D. Lee, J. Livingood, Experimental flow characteristics of a single turbulent jet impinging on a flat plate, (1970).

[19] Y. Kamotani, I. Greber, Experiments on a turbulent jet in a cross flow, AIAA J. 10 (1972) 1425–1429.
[20] C.D. Donaldson, R.S. Snedeker, D.P. Margolis, A study of free jet impingement. Part 2. Free jet turbulent structure and impingement heat transfer, J. Fluid Mech. 45 (1971) 477–512.
[21] J. Vlachopoulos, J.F. Tomich, Heat transfer from a turbulent hot air jet impinging normally on a flat plate, Can. J. Chem. Eng. 49 (1971) 462–466. doi:10.1002/cjce.5450490406.
[22] J. Vlachopoulos, Velocity and temperature profiles in compressible turbulent wall jets, Can. J. Chem. Eng. 49 (1971) 44–50.
[23] Y. ERA, A. Saima, An Investigation of Impinging Jet: Experiments by Air, Hot Air and Carbondioxide, Bull. JSME. 19 (1976) 800–807.
[24] G.J. Borell, T.E. Diller, A Convection Calibration Method for Local Heat Flux Gages, J. Heat Transf. 109 (1987) 83–89. doi:10.1115/1.3248073.
[25] P. Tie, Q. Li, Y. Xuan, Investigation on the submerged liquid jet arrays impingement cooling, Appl. Therm. Eng. 31 (2011) 2757–2763. doi:10.1016/j.applthermaleng.2011.04.048.
[26] K. Wilber, J. Maulbetsch, Air-Cooled Condenser Design, Specification, and Operation Guidelines, EPRI, Palo Alto, CA: 2005. 1007688, (2005).
[27] SPX COOLING TECHNOLOGIES, INC., Cooling Tower Energy and Its Management, (2016). http://spxcooling.com/.

Paper 2: Experimental Study of an Array of Jets Impinging on a Constant Temperature Surface with Rectangular Grooves Part-I: Dry Conditions

Abdulmohsen Alsaiari

Department of Mechanical Engineering, Virginia Tech, Heat Transfer Measurements Laboratory, 338 Goodwin Hall, 635 Prices Fork Road Blacksburg – MC 0238, VA 24061; aoa212@vt.edu

Abdulrahman Alghamdi

Department of Mechanical Engineering, Virginia Tech, Heat Transfer Measurements Laboratory, 338 Goodwin Hall, 635 Prices Fork Road Blacksburg – MC 0238, VA 24061; bosha18@vt.edu

Holly Leonard

Department of Mechanical Engineering, Virginia Tech, Heat Transfer Measurements Laboratory, 338 Goodwin Hall, 635 Prices Fork Road Blacksburg – MC 0238, VA 24061; holly95@vt.edu

Thomas E. Diller*

Department of Mechanical Engineering, Virginia Tech, 313C Goodwin Hall, 635 Prices Fork Road – MC 0238, Blacksburg, VA 24061; tdiller@vt.edu

Abstract

An experimental study of an array of jets impinging of a constant temperature surface with rectangular grooves was conducted. A constant temperature heated grooved plate was subjected to vertical jets of air pressurized out of orifices. Power and temperature measurements were performed to obtain heat transfer convection coefficients. The objective is to characterize the resulting heat transfer under varying operation conditions such as array orifices diameter, array to surface stand-off distance, flow open area percentage, groove width and depth, and jet relative position to the groove. Results showed 10%~55% improvement in heat transfer when compared to a flat surface. Improvement percentage tends to be higher at wider gaps between the array of

orifices and the grooved surface. An improvement of 30%~40% was observed when increasing Re either by increasing orifice diameter or jet speed. Similar improvement was observed at higher flow open area percentages. No significant change in heat transfer resulted from decreasing the size of the grooves from 3.56mm to 2.54mm. Similarly, no noticeable change in heat transfer resulted from changing the relative position of the jets striking the surface at the top of the grooves to the bottom of the grooves. Deeper grooves with twice the depth gave statistically similar average heat transfer coefficients as shallower grooves.

2.1 Introduction

Jet impingement heat transfer is utilized in many industrial applications where high convective heat transfer coefficients are of interest. The advantage of impinging jets is the thin boundary layers in stagnation regions. This creates higher heat transfer coefficient on the surface with comparable flow rates and fan power. Surface alterations is one way of enhancing jet impingement heat transfer. Examples of such alterations in the literature are numerous and include ribbed [1–4], dimpled [5–8], pinned [9–12], or porous [13,14] target surfaces. The different types of alterations are dictated by the application relevant to the study. A single jet [15,16] or an array of jets [17,18] can be used in combination with a surface with rectangular ribs or grooves. The ribs provide extra surface area for heat transfer and promote flow turbulence and the generation of secondary flows; which are aspects expected to increase heat transfer. Gau et al. [15] studied a single slot jet impinging on surface with rectangular rips without induced crossflow. They reported that heat transfer decreased compared to the flat case due to stagnant air bubble formation between the ribs as result of the narrow space between the ribs. Haiping et al. [18] studied an array of circular jets striking a surface with rectangular ribs with induced crossflow. They reported that heat transfer decreased due to loss of momentum in the wall jet resulting from the grooves

obstructing flow. Therefore, improvement in heat transfer is not always expected due to grooves on the surface as reported in [2,19–21].

A number of factors affect heat transfer resulting from jet impingement on a surface with rectangular grooves or ribs. At low crossflow conditions, Gau et al. [15] reported that a turbulent jet at higher H/d > 8 penetrated the stagnant air bubbles formed between the grooves and heat transfer increased. However, increased H/d ratio at high cross flow conditions resulted in decreased heat transfer [22]. The shape, depth, width and alignment of the ribs have been reported to affect the heat transfer of jet impingement. Son et al. [21] observed that for an array of jets at high crossflow conditions, sharp edged ribs have more enhancement compared to filleted ribs. The shape of the rib can cause the jet to rebound from the surface after it strikes it causing a decrease in heat transfer as was observed in[15,23]. Haiping et al. [22] reported that smaller groove width with small pitch-to-height ratios were observed to increase heat transfer due to their increased inducement of flow circulation within the grooves. They also found that deeper grooves with small slot width-to-rib height ratio have insignificant effect on heat transfer at high crossflow conditions. However, without induced crossflow, deeper grooves were found to adversely affect heat transfer due to the hindering of the wall jet [15]. Son et al. [21] reported that streamwise aligned ribs resulted in lower heat transfer compared to a flat surface. Liu et al.[4] observed that transversely aligned grooves resulted on slightly higher heat transfer compared to longitudinal grooves. They attributed this finding to flow circulation near the groove edges. The relative position of a jet to the rib can change the resulting heat transfer. Haiping et al in [18] showed that the jet impingement in the center between two ribs resulted in the best heat transfer enhancement for widely spaced ribs with or without initial crossflow. However, no significant change was observed in heat transfer

between the jet stagnating at the top of the rib or in between two ribs for conditions of small grooves width and/or higher ratios of H/d [15].

The above-mentioned observations illustrate the complex nature of jet impingement with surface alterations. Therefore, most of the conducted research is of an experimental approach and correlations are limited to specific geometries and arrangements. The current study addresses the problem of different arrays of circular jets impinging on a surface with rectangularly grooved channels. Two possible applications are condensers in thermal power plants and Vapor-Compression refrigeration cycles. A previous published paper demonstrated the potential of jet impingement for condensers [24]. The aim of the current study is to characterize heat transfer and important factors of arrays of round jets impinging on a surface with rectangular grooves on a dry condition.

2.2 Experimental Setup

2.2.1 Apparatus

The experimental apparatus for measuring the average surface heat transfer is depicted in figure 2.1. A wind tunnel was used to supply air for the experiment at varying jet speeds by regulating the power supplied to an axial flow fan. A manometer was used to measure the static pressure in a vicinity of the orifice opening inside the plenum, though not shown in the figure. Appropriate Δp was maintained to satisfy the required jet speed as described by the Bernoulli equation:

$$U_o = \sqrt{\frac{2\Delta p}{\rho}} \tag{1}$$

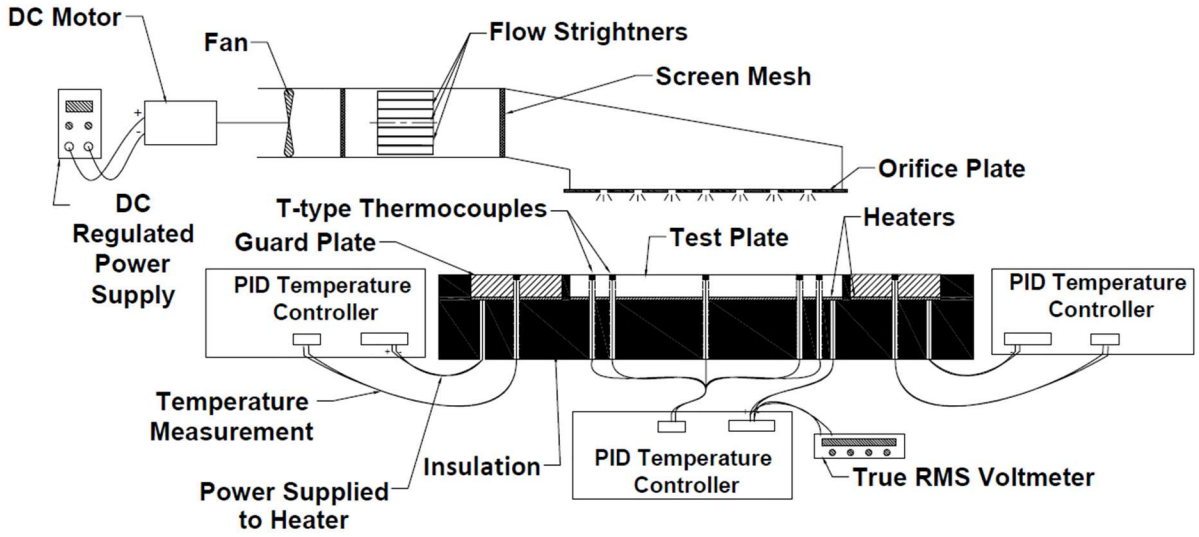

Figure 2. 1: *Abstract depiction of the experiment apparatus.*

Six different jet arrays were made by drilling circular holes in 1.6 mm (1/16") aluminum plates. The open area A_o percentage is the ratio between the area of the orifices and the test plate surface area. The additional side surface area of the grooves are not included and A_o is calculated as:

$$A_o = \frac{C_D \cdot N \cdot \frac{\pi}{4} d^2}{A_S} \tag{2}$$

Where N is the total number of jets in the array and C_D is the discharge coefficient.

As shown in figure 2.2, three of the arrays, a to c, have the same value of the open area A_o =1.5% but at different orifice diameters of 3.18mm, 4.76mm, and 6.35mm. The diameter of orifices in the remaining arrays, d to f, was fixed at 4.76mm while the value of A_o was varied with values of 1%, 2%, and 3%.

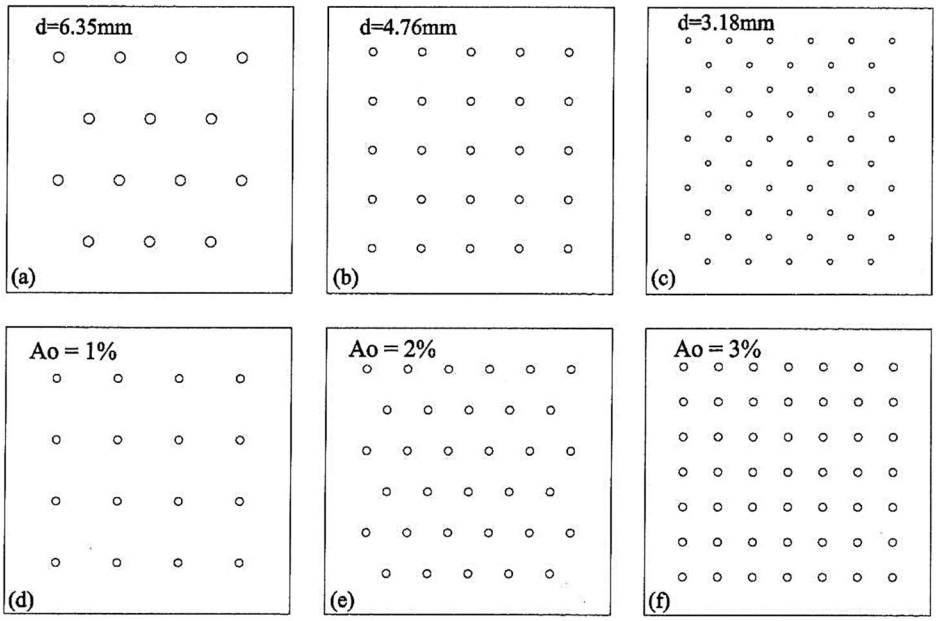

Figure 2. 2: *Jets array: (a) to (c), A_o=1.5% with different diameters, (d) to (f), d=4.76mm with variable A_o.*

The arrays were fabricated in a CNC mill to ensure that all orifices in each plate have the same geometrical characteristics.

Most jet arrays are produced using orifices in thin plates with discharge coefficients of C_D between 0.75 and 0.85, because of the contraction of the flow as it turns through the orifice. This gives an effective diameter of:

$$d_e = d\sqrt{C_D} \tag{3}$$

Although shown to be important to the resulting heat transfer [25], many jet array studies overlook this effect. To measure C_D, water flow was used for a sample of n orifices in each array. The Reynolds number based on the orifice diameter Re_d was used to match air and water velocities. Reynolds number ranged from 4,070 to 12,210. The corresponding water head was maintained at a prescribed level by regulating water flow to the container with the orifice plate beneath it. Water was allowed to flow through the selected orifice and the flow rate of water $\dot{m}_w$ was measured using an electronic weight scale and a timer. The discharge coefficient then was calculated as:

$$C_D = \frac{\dot{m}_w}{\rho_w \cdot \frac{\pi}{4} \cdot d^2 \cdot {U_{o,w}}^2} \quad (4)$$

Table 1 shows the measured discharge coefficients for the three different orifice sizes and resulting effective diameter. Cd was observed to be independent of Re_d.

Table 2. 1*: Discharge coefficients, CD*

d(mm)	n	C_D	C_D standard deviation	d_e(mm)
3.18	6	0.784	0.003	2.81
4.76	6	0.785	0.005	4.22
6.35	6	0.802	0.002	5.69

2.2.2 Test Plates

The air jets cooled the test surface which was heated electrically. The steady state power measurements were used to calculate the average heat transfer coefficients. Three different 152.4mm by 152.4mm grooved aluminum plates, that each has a thickness of 12.7 mm, were tested and compared to the flat surface. Rectangular grooves were milled on to the surface of each plate with different dimensions as shown in figure 2.3. The majority of experiments were performed with plate (b) in which each groove has a width and depth of 3.56mm and length of 147.3mm. This created 21 protruding ribs with a height of 3.56mm aligned transversely as shown in figure 2.4. Plates (a) and (c) were used to examine the effect of depth and width of the grooves on heat transfer. Plate (c) has grooves with the same width and length as but with a depth of 7.11mm. Plate (a) has grooves with the same depth and length as the plate (b) but a narrower width of 2.54mm. Plates (b) and (c) have the same number of grooves, but the plate (a) geometry results in 30 grooves.

A flat surface of 152.4mm by 152.4mm gives an area of 0.023 m^2. The increase in surface area resulting from the grooves is 140% in plate (a), 95% in plate (b), and 194% in plate (c) of the

flat plate surface. The reflection of such increase in surface area on heat transfer will be examined in the results section.

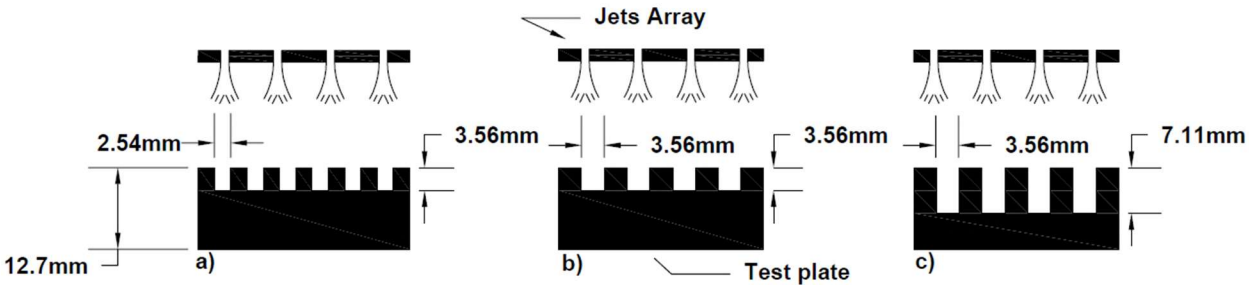

Figure 2. 3: *Test plates: a) Width=2.54mm and depth=3.556, b) Width and depth=3.556mm a) Width=3.556mm depth=7.11mm.*

A total of 14 T-type thermocouples were distributed and press fit into test plate b in different locations as shown in figure 2.4. A number of the thermocouples were fitted on the bottom of the grooves and some in the top of the ribs to ensure uniformity of temperature measurement. Eight of the thermocouples were wired in parallel and supplied to a Eurotherm 810 PID temperature controller. The controller was used with a Eurotherm 831 Silicon Control Rectifier (SCR) to supply power to the heater. Therefore, it is necessary to use a true-RMS voltmeter (HP-3486A) to measure the voltage to determine the power supplied to the heater. Once voltage was measured, the power was calculated as:

$$\mathcal{P} = \frac{V^2}{\mathcal{R}} \tag{5}$$

Where $\mathcal{R}$ is the electrical resistance of the heater, which was constant with temperature over operating range. Temperature readings from the remaining six thermocouples were recorded individually using an NI-9214 DAQ system. To minimize edge losses, four guard plates surrounded the test plate and were maintained at the same set-point temperature as the test plate using additional PID controllers and SCR's. The test plate and the guard plates were placed on a multilayer of insulation materials of wood and fiberglass to minimize the conduction losses.

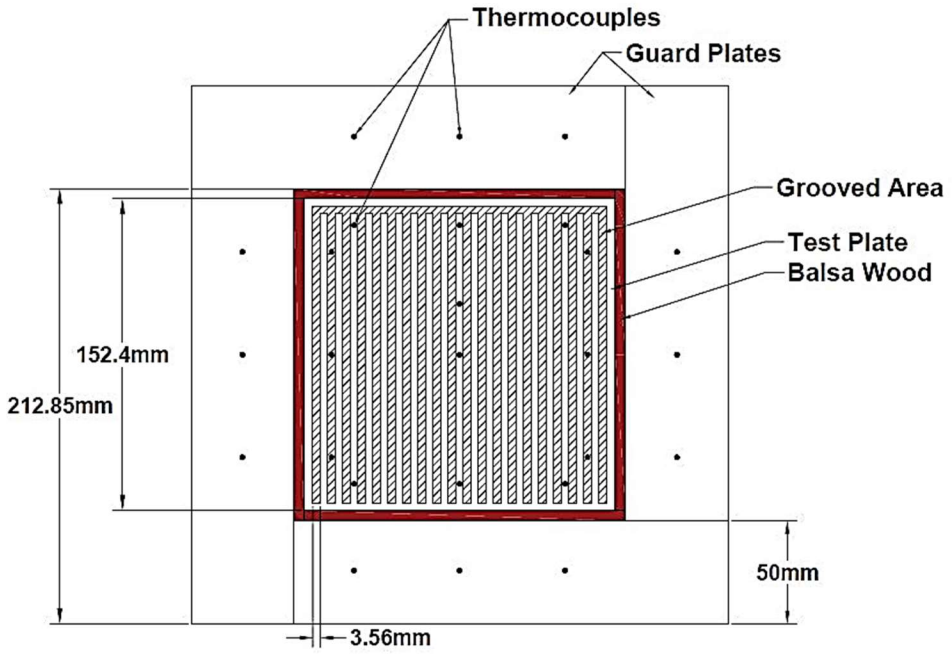

Figure 2. 4*: Top view of test Plates b with guard plates and thermocouples locations.*

2.2.3 Test Procedure and Data Processing

The majority of the experiments were performed on test plate (b) in figure 2.3. For each array in figure 2.2, jet velocities of 5m/s, 7.5m/s, 10m/s, and 20m/s were used with three stand-off distance ratios H/d_e of 5.4, 7.18, and 12. This results in a total of 72 experiments performed on test plate (b). This is compared to 132 experiments that were performed on the flat surface in [24]. Twenty experiments were performed on plates (a) and (c) to examine the effect of width and depth of the grooves on heat transfer.

At prescribed test parameters mentioned above, average heat transfer coefficients were obtained through the measurement of power supplied to the heater. The power was controlled to sustain the surface temperature T_s of the test plate through controlling voltage supplied to the heater. The test plate typically requires 25 minutes to reach steady constant surface temperature, when T_s, T_o, and V are recorded. Surface temperature T_s was obtained by averaging temperature readings of six thermocouples uniformly distributed on the test surface. A standard deviation of

1.5°C was observed on T_s readings across the plate spatially. Accordingly, the surface temperature can be treated as uniform. The ambient temperature T_o was logged using a thermocouple placed inside the wind tunnel.

The power at steady state was obtained using equation 1. Accounting for the conduction and radiation losses, the convection heat flux from the surface is calculated as:

$$q^{"}_{conv} = \frac{\mathcal{P}}{A_s} - q^{"}_{cond} - q^{"}_{rad} \quad (6)$$

Where A_s is the test plate projected surface area of 152.4mm by 152.4mm as shown in figure 2.4. This area does not include the side surface area of the ribs. Accordingly, the average convection heat transfer coefficient is obtained as:

$$h = \frac{q^{"}_{conv}}{T_s - T_o} \quad (7)$$

The corresponding Nusselt number is:

$$Nu = \frac{h \cdot d_e}{k} \quad (8)$$

A total of 36 measurements of Nu were performed at each test conditions.

The conduction heat losses $q^{"}_{cond}$ were divided into lateral loss and downward loss. The lateral loss was significantly diminished due to the use of four guard plates surrounding the test plate and the loss was neglected. The downward loss was estimated as 1% of the power dissipated by the heater. This estimation was obtained through thermal resistances analysis for the upward and downward mediums enclosing the heater. The radiation loss was calculated, assuming the surrounding is at the initial jet temperature, as:

$$q^{"}_{rad} = \varepsilon\sigma(T_s^4 - T_o^4) \quad (9)$$

The surface emissivity ε value was found to be 0.76 with a standard deviation of ± 0.03. This estimation was obtained by using FLIR SC600 Series High-Resolution LWIR Science-Grade

infrared camera where a portion of the test plate was painted with a black paint with a known value of ε_b= 0.94, while another portion remained unpainted. The emissivity of the plate was obtained as:

$$\varepsilon = \frac{T^4{}_{unpainted}}{T^4{}_b} \cdot \varepsilon_b \tag{10}$$

Accordingly, the percentage of heat transfer due to radiation was found to vary from 2.5% to 7% of $\mathcal{P}$ depending on the magnitude of the convection portion of heat transfer.

2.2.4 Data Statistics and Uncertainty

Confidence intervals were constructed for the measured values of Nu. For each test, 36 measurements of Nu were recorded giving the mean value, standard deviation, and the 95% confidence interval. It was observed that the size of the confidence interval varied between 4% to 5% of the estimated mean value of Nu.

The sources of uncertainty in the measurement of Nu are listed in table. 2 with the respective uncertainty values. Parameters were selected based on the expression that was adopted to calculate Nu through the measurement of Voltage V, electrical resistance $\mathcal{R}$, and temperature T. The average Nusselt number Nu was obtained as:

$$Nu = \frac{h\, d_e}{k} = \frac{V^2/\mathcal{R}}{(T_s - T_o)A_s} \cdot \frac{d_e}{k} \tag{11}$$

Therefore, the uncertainty on Nu_{av} was estimated as:

$$U_{n_{(Nu)}} = \left\{ \left[\frac{\partial}{\partial V}(Nu) \cdot U_{n_V}\right]^2 + \left[\frac{\partial}{\partial \mathcal{R}}(Nu) \cdot U_{n_{\mathcal{R}}}\right]^2 + \left[\frac{\partial}{\partial d_e}(Nu) \cdot U_{n_{d_e}}\right]^2 + \left[\frac{\partial}{\partial T}(Nu) \cdot U_{n_T}\right]^2 + \right.$$

$$\left. \left[\frac{\partial}{\partial A_s}(Nu) \cdot U_{n_{A_s}}\right]^2 + \left[\frac{\partial}{\partial k}(Nu) \cdot U_{n_k}\right]^2 \right\}^{\frac{1}{2}} \tag{12}$$

The resulting value of estimated uncertainty Nu_{av} was 7%.

The 5% confidence interval value of the data and the 7% estimated uncertainty of the Nu are both indicators of the quality of the experiment and of the results produced.

Table 2. 2*: Sources of uncertainty for the grooved surface.*

#	Source of uncertainty	Value	Unit
1	Voltage measurement, U_{n_V}	0.02% of measured V	volt
2	Resistance measurement, $U_{n_{\mathcal{R}}}$	0.5% of of measured $\mathcal{R}$	ohm
3	Temperature measurement, U_{n_T}	1.5	K
4	Surface area measurement, $U_{n_{A_s}}$	3.4×10^{-4}	m^2
5	Thermal conductivity value, U_{n_k}	1.3×10^{-4}	W/(m-K)
6	Orifice diameter measurement, $U_{n_{d_e}}$	4×10^{-5}	m

2.3 Results and Discussion

Experiments were performed at constant surface temperature T_s=42.8°C at which average convection heat transfer coefficients were obtained using equation 7. The measured convection coefficients are then compared to the coefficients measured at the flat surface in [24] each under respective test conditions. The ratio of diameter to groove depth d_e/e is 1.6 for array (a), 1.2 for arrays (b, d, e, and f) and 0.8 for array (c). See figure 2.2 for arrays.

Figure 2.7, 2.9, and 2.11 depicts the variation of the average Nusselt number for the flat surface Nu_{flat} with Re_{de} for fixed A_o = 1.5% and varying H/d_e. d_e is 2.81mm for figure 2.7, 4.22mm for figure 2.9, and 5.69mm for figure 2.11. Figures 2.8, 2.10, and 2.12 show the improvement in heat transfer for grooved test plate (b) by plotting the ratio of $Nu_{grooved}/Nu_{flat}$ versus Re_{de}. Figure 2.13, 2.15, and 2.17 depicts the variation of the average Nusselt number for the flat surface Nu_{flat} with Re_{de} for fixed d_e = 4.22mm and varying H/d_e. A_o is 1% for figure 2.13, 2% for figure 2.15, and 3% for figure 2.17. Reynolds number Re_{de} is calculated based on the effective diameter d_e and jet velocity. Experimental uncertainty is represented by bars plotted on each measurement.

2.3.1 The Effect of H/d_e

Figures 2.5, 2.7, and 2.9 show the variation of Nu with Re_{de} for the flat surface at different H/d_e ratios. The A_o=1.5% for the figures, however, d_e is different for each figure as denoted. The figures show that Nu_{flat} increases with increasing Re_{de} and decreases with increasing H/d_e ratio. Nu_{flat} is slightly higher for d_e=2.81mm as compared to d_e=5.69mm under similar Re_{de} and H/d_e. Similar trends were observed for $Nu_{grooved}$ to increase with increasing Re_{de} and decrease with increasing H/d_e ratio. Heat transfer improved for the grooved surface when compared with the heat transfer of the flat plate as shown in figures 2.6, 2.8, and 2.10. A trend of higher improvement of heat transfer ranging from 40%~60% was observed at H/d_e =12. Higher improvement of heat transfer of is also observed at increasing Re at H/d_e = 7.18 compared to H/de = 5.4. The latter two observations can be attributed to the lower prospect of stagnant air bubbles formation inside the grooves at higher H/d_e ratio as observed by Gau et al. [15]. They reported that at high H/d_e ratio the jet strikes the surface with higher level of turbulence causing the penetration of stagnant air bubbles inside the grooves. Such penetration promotes high momentum transfer and flow circulation inside the grooves and enhances heat transfer. However, in the case of low H/d_e ratio, the stagnant air bubbles form inside the grooves hindering momentum transfer and flow circulation and resulting in lower enhancement.

2.3.2 The Effect of Diameter d_e

The ratio of diameter to groove width d_e/p = 0.8 for figure 2.6, and d_e/p = 1.6 for figure 2.10. Figure 2.6 shows a decreasing trend in the improvement of heat transfer verses Re_{de} especially at low H/d_e. Such decrease can be attributed to increased obstruction by the ribs to the wall jet. This obstruction is because that the ribs becomes large relative to the jet causing enhance

loss in momentum [23]. The decrease in improvement is mitigated and reversed as d_e/p increases at which improvement becomes less sensitive to Re_{de} as shown in figure 2.10.

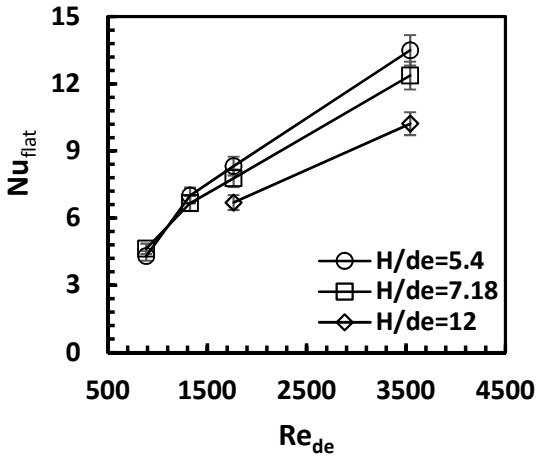

Figure 2. 5: *Variation of Nu vs Re_{de} for the flat plate, d_e=2.81mm, and A_o=1.5%.*

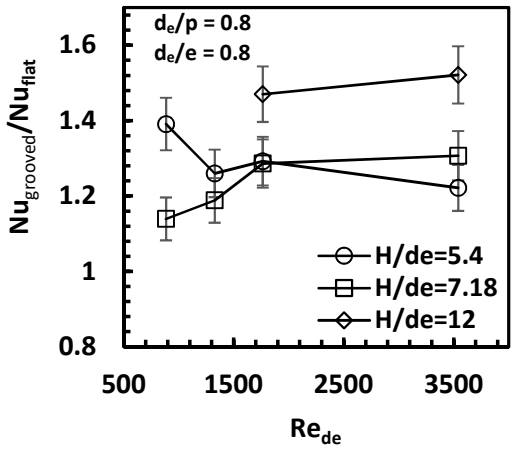

Figure 2. 6: *Improvement on Nu due to grooves vs Re_{de} d_e=2.81mm, and A_o=1.5%.*

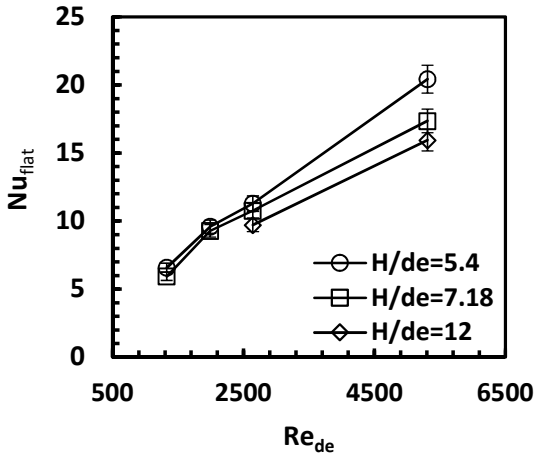

Figure 2. 7: *Variation of Nu vs Re_{de} for the flat plate, d_e=4.22mm, and A_o=1.5%.*

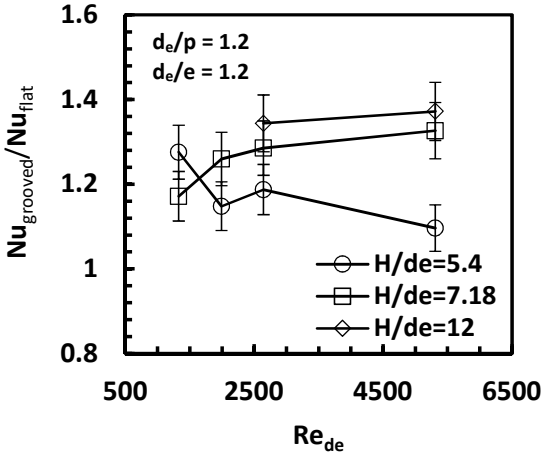

Figure 2. 8: *Improvement on Nu due to grooves vs Re_{de} d_e=4.22mm, and A_o=1.5%.*

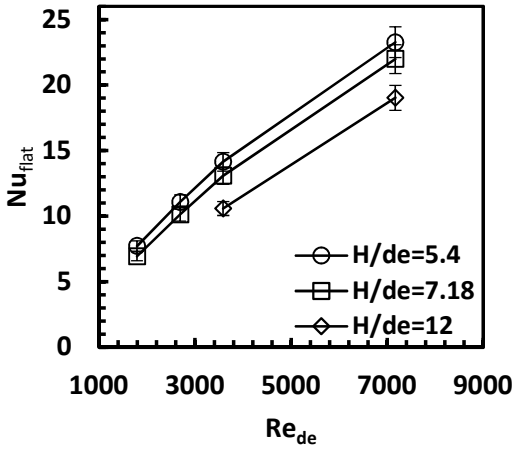

Figure 2. 9: *Variation of Nu vs Re_{de} for the flat plate, d_e=5.69mm and A_o=1.5%.*

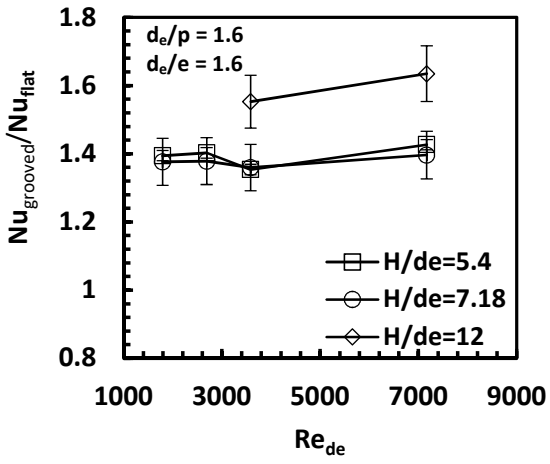

Figure 2. 10: *Improvement on Nu due to grooves vs Re_{de} for d_e=5.69mm, and A_o=1.5%.*

2.3.3 The Effect of A_o

Figures 2.11, 2.13, and 2.15 shows the variation of Nu with Re_{de} for the flat surface at different H/d_e ratios. The de=4.22mm for the figures, however, A_o is different for each figure as denoted. The figures show that Nu_{flat} increases with increasing Re_{de} and decreases with increasing H/d_e ratio. Nu_{flat} is higher for A_o=3% as compared to A_o=1% under similar Re_{de} and H/d_e. Similar trends were observed for $Nu_{grooved}$ to increase with increasing Re_{de} and increasing A_o and decrease with increasing H/d_e ratio. Heat transfer improved for the grooved surface when compared with the heat transfer of the flat plate as shown in figures 2.12, 2.14, and 2.16. A trend of higher improvement in heat transfer at H/d_e = 12 was observed at all A_o values. It can be deduced from figurers 2.12, 2.14, and 2.16 that $Nu_{flat}/Nu_{grooved}$ is slightly higher at A_o=3% compared to A_o=1%, and 2%. This can be attributed to the higher crossflow resulting from increased flow rate at A_o=3%. Another observation is the insensitivity of improvement in heat transfer to increased Re_{de} at A_o=3%.

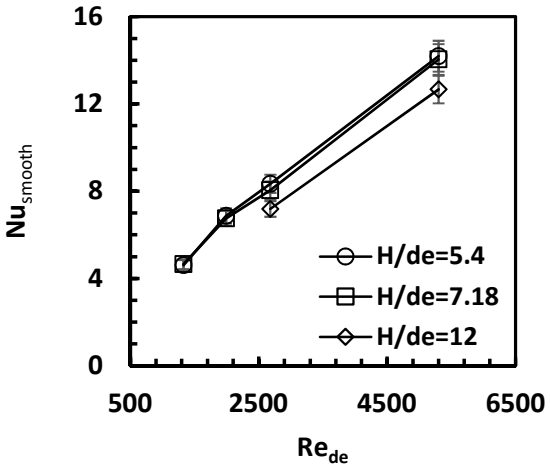

Figure 2. 11*: Variation of Nu vs Re_{de} for the flat plate at A_o=1% and d_e=4.22mm.*

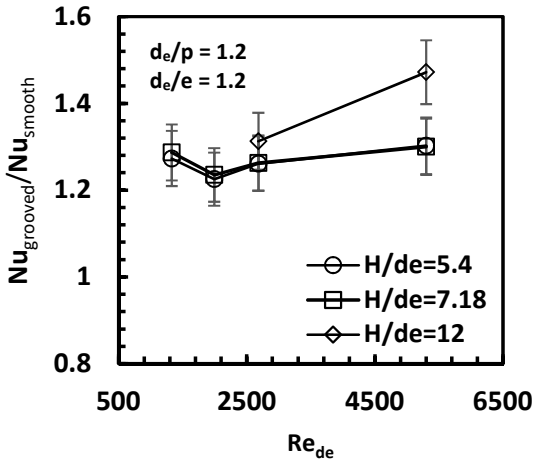

Figure 2. 12*: Improvement on Nu due to grooves vs Re_{de} at A_o=1% and d_e=4.22mm.*

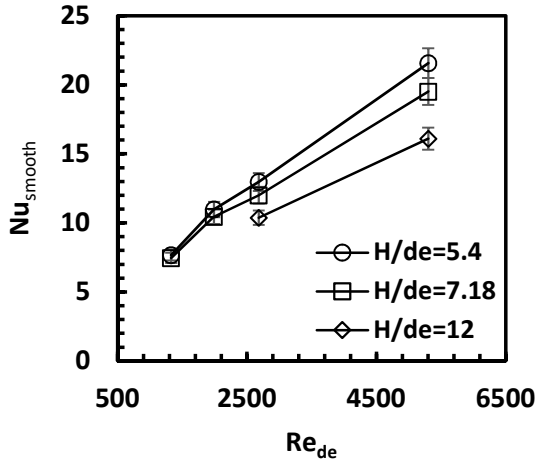

Figure 2. 13*: Variation of Nu vs Re_{de} for the flat plate at A_o=2% and d_e=4.22mm.*

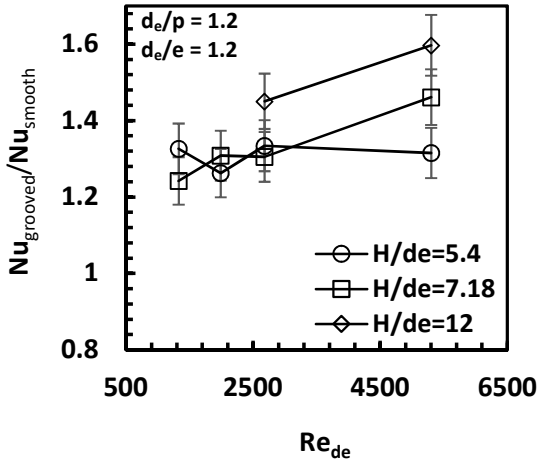

Figure 2. 14*: Improvement on Nu due to grooves vs Re_{de} at A_o=2% and d_e=4.22mm.*

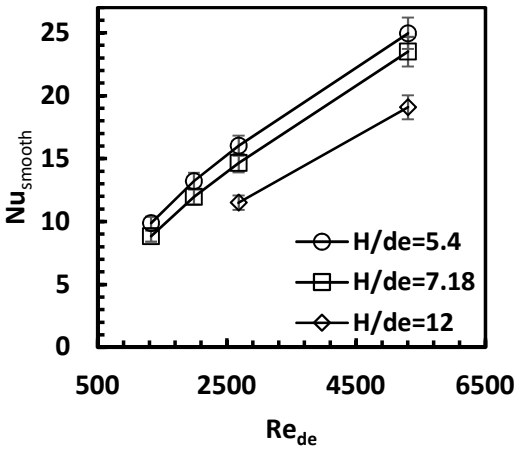

Figure 2. 15*: Variation of Nu vs Re_{de} for the flat plate at A_o=3% and d_e=4.22mm.*

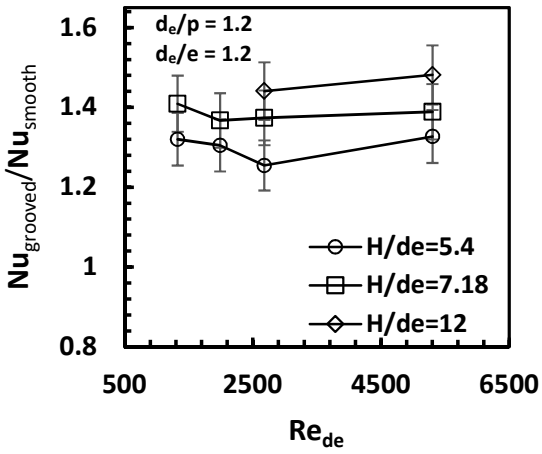

Figure 2. 16*: Improvement on Nu due to grooves vs Re_{de} at A_o=3% and d_e=4.22mm.*

2.3.4 The Effect of Jet Position

To examine the effect of the position of the jets relative to the grooves on heat number of experiments were performed with two different position arrangements. Jet array (e) with A_o = 1% and d_e = 4.22mm was used with test plate (b). In the first arrangement, the orifices of the array were aligned in a position that allows the jets to impinge between the two grooves i.e. on the top of the ribs. In the second, the jets impinged on the middle of the grooves i.e. between two ribs. Figure 2.17 shows the variation of Nusselt number with H/d_e for the above-mentioned arrangements with uncertainty represented by bar on each measurement. The figure shows that the results of the two different arrangements are statistically similar. Uncertainty is represented by bars placed on each measurement in the figure.

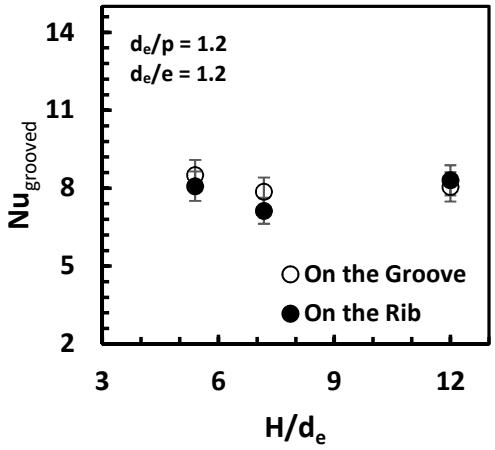

Figure 2. 17: *$Nu_{grooved}$ vs H/d_e at A_o = 1%, d_e=4.22mm and Re_{de}=1992*

2.3.5 The Effect of Groove Geometry

The groove width on test plate (a) in figure 2.3 is 2.55mm. The plate was used with jet array (e) in figure 2.2 of A_o = 1% and de = 4.22mm to examine the effect of groove width on heat transfer. The results are shown in figure 2.18 where the variation of Nusselt number is plotted versus H/d_e at different Re_{de} values. It can be deduced that narrower grooves did not result in statistically significant changes in heat transfer. Therefore, the width of the grooves has no significant effect on heat transfer for the above-mentioned arrangement of jets array and grooved plat. Uncertainty is represented by bars placed on each measurement in the figure.

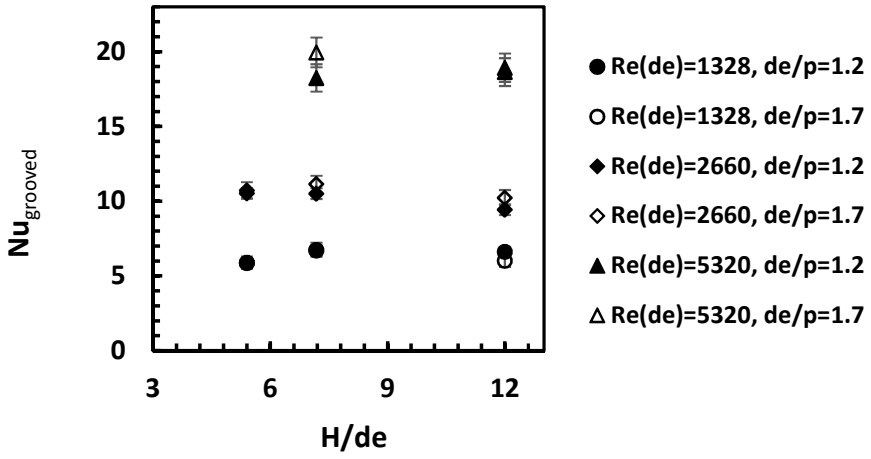

Figure 2. 18: *$Nu_{grooved}$ vs H/d_e at A_o = 1% and d_e=4.22mm*

The effect of grooves depth on heat transfer is depicted in figure 2.19 which shows the average Nusselt number verses H/d_e at two Re_{de} for jets arrays (a) and (c) each was used with test plate (b). Both jet arrays have A_o = 1.5% but d_e = 5.69mm for array (a) and d_e = 2.81mm for array (c). A slight increase in $Nu_{grooved}$ is observed when groove depth increases from 3.56mm to 7.11mm. The increase in heat transfer is apparent at lower H/d_e values of 5.4 and 7.18 compared to H/de =12. However, the increase in heat transfer is insignificant and falls within the uncertainty limits of the measurement. Uncertainty is represented by bars placed on each measurement in the figure.

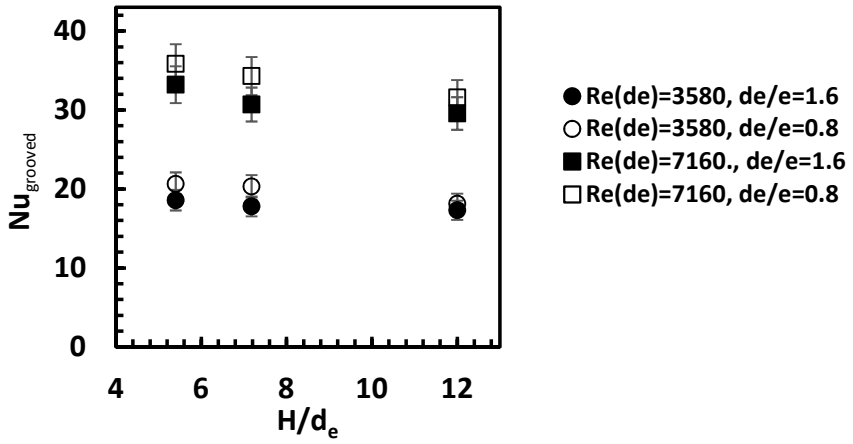

Figure 2. 19: *$Nu_{grooved}$ vs H/d_e at A_o = 1.5%, test plate (b), and jets array (a) and (c).*

2.4 Conclusion

Array jet impingement on a constant temperature surface with rectangular grooves resulted in enhancement of heat transfer in comparison to impingement on flat surface. This was observed experimentally in this study with result uncertainty of 7%. The increase in surface area due to the

grooves ranged from 95% to 194%, depending on the geometry, in comparison to the flat surface. However, heat transfer enhancement due to the grooves only ranged from 15% to 63% when compared to the flat surface results. Higher percentage of enhancement in heat transfer was observed in conditions of high H/d_e ratios, large orifice diameters, and jet velocities. The relative position of the jets to the grooves showed no statistically significant effect on heat transfer. Examination of the effect of groove width and groove depth on heat transfer showed the effects to be insignificant. In a future study, similar approach will be followed but with the grooves containing water. The knowledge of the convection heat transfer will enable calculating evaporation rates. Therefore, the current study represents a rational intermediate step for the future study of jet impingement of a grooved surface containing water.

Nomenclatures

A	Area(m^2)
d	Diameter(m)
e	Groove depth
H	Orifice to surface distance(m)
k	Thermal conductivity($W/m\text{-}\ ^oC$)
$\dot{m}$	Mass flow rate(kg/s)
p	Groove width
q”	Heat flux(W/m^2)
$\mathcal{R}$	Electrical resistance(ohm)
T	Temperature(^oC)
U	Velocity(m/s)
$U_{n_{A_s}}$	Uncertainty in surface area(m^2)
$U_{n_{d_e}}$	Uncertainty in diameter(m)
U_{n_k}	Uncertainty in thermal conductivity($W/m\text{-}\ ^oC$)
$U_{n_{\mathcal{R}}}$	Uncertainty in eelectrical resistance(ohm)
U_{n_V}	Uncertainty in voltage (volts)
V	Voltage (volts)
υ	Kinematic viscosity
Δp	Pressure difference(Pa)
ρ	Density(kg/m^3)
σ	Stefan-Boltzmann constant ($\sigma = 5.66961 \times 10^{-8}\ W/m^2 \cdot K^4$)

Non-dimensional

A_o	Open area percentage(%)
ε	Emissivity
N	Number of Jets
Nu	Nusselt number ($h \cdot d_e/k$)
n	Number of experiments
$U_{n_{(Nu)}}$	Uncertainity in Nusselt number
Re_{de}	Reynolds number ($U_o \cdot d_e/v$)
Subscripts	
b	Black body property
cond	Conduction
conv	Convection
grooved	Grooved surface property
o	Jet exit property
rad	Radiation
s	Surface Property
w	Water

References

[1] L.M. Su, S.W. Chang, Detailed heat transfer measurements of impinging jet arrays issued from grooved surfaces, Int. J. Therm. Sci. 41 (2002) 823–841. doi:10.1016/S1290-0729(02)01377-7.

[2] T.A. Trabold, N.T. Obot, Impingement Heat Transfer Within Arrays of Circular Jets: Part II—Effects of Crossflow in the Presence of Roughness Elements, J. Turbomach. 109 (1987) 594–601. doi:10.1115/1.3262153.

[3] L. Tan, J.-Z. Zhang, H.-S. Xu, Jet impingement on a rib-roughened wall inside semi-confined channel, Int. J. Therm. Sci. 86 (2014) 210–218. doi:10.1016/j.ijthermalsci.2014.06.037.

[4] Y.-H. Liu, S.-J. Song, Y.-H. Lo, Jet impingement heat transfer on target surfaces with longitudinal and transverse grooves, Int. J. Heat Mass Transf. 58 (2013) 292–299. doi:10.1016/j.ijheatmasstransfer.2012.11.042.

[5] S.V. Ekkad, D. Kontrovitz, Jet impingement heat transfer on dimpled target surfaces, Int. J. Heat Fluid Flow. 23 (2002) 22–28. doi:10.1016/S0142-727X(01)00139-4.

[6] K. Kanokjaruvijit, R.F. Martinez-botas, Jet impingement on a dimpled surface with different crossflow schemes, Int. J. Heat Mass Transf. 48 (2005) 161–170. doi:10.1016/j.ijheatmasstransfer.2004.08.005.

[7] G.S. Azad, Y. Huang, J.-C. Han, Impingement Heat Transfer on Dimpled Surfaces Using a Transient Liquid Crystal Technique, J. Thermophys. Heat Transf. 14 (2000) 186–193. doi:10.2514/2.6530.

[8] Z. Shen, Q. Jing, Y. Xie, D. Zhang, Thermal Performance of Miniscale Heat Sink With Jet Impingement and Dimple/Protrusion Structure, J. Heat Transf. 139 (2017) 52202-52202–8. doi:10.1115/1.4036035.

[9] M. Farhad Ismail, S.C. Saha, Enhancement of Confined Air Jet Impingement Heat Transfer Using Perforated Pin-Fin Heat Sinks, in: M.M.K. Khan, A.A. Chowdhury, N.M.S. Hassan (Eds.), Appl. Thermo-Fluid Process. Energy Syst. Key Issues Recent Dev. Sustain. Future,

Springer Singapore, Singapore, 2018: pp. 231–243. https://doi.org/10.1007/978-981-10-0697-5_10.
[10] S. Ndao, Y. Peles, M.K. Jensen, Effects of pin fin shape and configuration on the single-phase heat transfer characteristics of jet impingement on micro pin fins, Int. J. Heat Mass Transf. 70 (2014) 856–863. doi:10.1016/j.ijheatmasstransfer.2013.11.062.
[11] A.M. El-Jummah, G.E. Andrews, J.E.J. Staggs, Enhancement of Impingement Heat Transfer With the Crossflow Normal to Ribs and Pins Between Each Row of Holes, (2018) V05AT10A006. doi:10.1115/GT2018-76969.
[12] Y. Rao, Y. Liu, C. Wan, Multiple-jet impingement heat transfer in double-wall cooling structures with pin fins and effusion holes, Int. J. Therm. Sci. 133 (2018) 106–119. doi:10.1016/j.ijthermalsci.2018.07.021.
[13] B. Buonomo, G. Lauriat, O. Manca, S. Nardini, Numerical investigation on laminar slot-jet impinging in a confined porous medium in local thermal non-equilibrium, Int. J. Heat Mass Transf. 98 (2016) 484–492. doi:10.1016/j.ijheatmasstransfer.2016.03.036.
[14] C. Zing, S. Mahjoob, Numerical Investigation of Thermal Transport in Confined Single and Multiple Jet Impingements Through Porous Filled Non-Uniform Cross Section Channels, in: 2018 17th IEEE Intersoc. Conf. Therm. Thermomechanical Phenom. Electron. Syst. ITherm, 2018: pp. 455–464. doi:10.1109/ITHERM.2018.8419595.
[15] C. Gau, C.C. Lee, Impingement cooling flow structure and heat transfer along rib-roughened walls, Int. J. Heat Mass Transf. 35 (1992) 3009–3020. doi:10.1016/0017-9310(92)90320-R.
[16] B. Sagot, G. Antonini, F. Buron, Enhancement of jet-to-wall heat transfer using axisymmetric grooved impinging plates, Int. J. Therm. Sci. 49 (2010) 1026–1030. doi:10.1016/j.ijthermalsci.2009.12.011.
[17] Y. Xing, B. Weigand, Experimental Investigation on Staggered Impingement Heat Transfer on a Rib Roughened Plate With Different Crossflow Schemes, (2010) 1–11. doi:10.1115/GT2010-22043.
[18] C. Haiping, Z. Dalin, H. Taiping, Impingement Heat Transfer From Rib Roughened Surface Within Arrays of Circular Jet: The Effect of the Relative Position of the Jet Hole to the Ribs, (1997) V003T09A067. doi:10.1115/97-GT-331.
[19] W.M. Yan, S.C. Mei, Measurement of detailed heat transfer along rib-roughened surface under arrays of impinging elliptic jets, Int. J. Heat Mass Transf. 49 (2006) 159–170. doi:10.1016/j.ijheatmasstransfer.2005.07.043.
[20] W.M. Yan, H.C. Liu, C.Y. Soong, W.-J. Yang, Experimental study of impinging heat transfer along rib-roughened walls by using transient liquid crystal technique, Int. J. Heat Mass Transf. 48 (2005) 2420–2428. doi:10.1016/j.ijheatmasstransfer.2004.12.048.
[21] C. Son, P. Ireland, D. Gillespie, The Effect of Roughness Element Fillet Radii on the Heat Transfer Enhancement in an Impingement Cooling System, (2005) 263–273. doi:10.1115/GT2005-68186.
[22] C. Haiping, Z. Jingyu, H. Taiping, Experimental Investigation on Impingement Heat Transfer From Rib Roughened Surface Within Arrays of Circular Jet: Effect of Geometric Parameters, (1998) V004T09A050. doi:10.1115/98-GT-208.
[23] C. Gau, I.C. Lee, Flow and impingement cooling heat transfer along triangular rib-roughened walls, Int. J. Heat Mass Transf. 43 (2000) 4405–4418. doi:10.1016/S0017-9310(00)00064-8.

[24] A. Alsaiari, Diller, Thomas E., Experimental Evaluation of Jet Impingement Cooling For Application in Power Plants Condensers, Am. Soc. Therm. Fluids Eng. (n.d.) 2377–2392. doi:10.1615/TFEC2017.iac.017571.
[25] P. Tie, Q. Li, Y. Xuan, Investigation on the submerged liquid jet arrays impingement cooling, Appl. Therm. Eng. 31 (2011) 2757–2763. doi:10.1016/j.applthermaleng.2011.04.048.

Paper 3: Experimental Study of an Array of Jets Impinging on a Surface with Rectangular Grooves Part-II: A Hybrid Wet/Dry Cooling Approach for Thermoelectric Power Plants Condensers

Abdulmohsen Alsaiari

Department of Mechanical Engineering, Virginia Tech, Heat Transfer Measurements Laboratory, 338 Goodwin Hall, 635 Prices Fork Road Blacksburg – MC 0238, VA 24061; aoa212@vt.edu

Abdulrahman Alghamdi

Department of Mechanical Engineering, Virginia Tech, Heat Transfer Measurements Laboratory, 338 Goodwin Hall, 635 Prices Fork Road Blacksburg – MC 0238, VA 24061; bosha18@vt.edu

Holly Leonard

Department of Mechanical Engineering, Virginia Tech, Heat Transfer Measurements Laboratory, 338 Goodwin Hall, 635 Prices Fork Road Blacksburg – MC 0238, VA 24061; holly95@vt.edu

Thomas E. Diller*

Department of Mechanical Engineering, Virginia Tech, 313C Goodwin Hall, 635 Prices Fork Road – MC 0238, Blacksburg, VA 24061; tdiller@vt.edu

Abstract

A hybrid cooling technique approach was proposed by using air jets impinging on a grooved surface with the grooves containing water. The approached is and evaluated experimentally for its feasibility as an alternative for cooling towers of thermoelectric power plants. Convection heat and mass transfer coefficients were measured experimentally for variety of operation conditions of surface temperature, jet speed, stand-off distance between surface and jets, and open area percentage. The heat and mass transfer analogy was successfully used to evaluate simultaneous heat and mass transfer. Results showed that hybrid jet impingement

provided high magnitudes of heat flux at low jet speeds and flow rates with values greater than 8,000W/m^2. Values of coefficient of performance, defined as the ratio of heat transfer to fan power, larger than 3,000 were achieved. This is an improved of 500% compared to jet impingement on a dry flat surface. The coefficient of performance of hybrid jet impingement is 600% to 1,500% more than air-cooled condensers and wet cooling towers. Water use for hybrid jet impingement cooling is efficient since evaporation energy is absorbed from the surface directly instead of cooling air to near wet-bulb temperature.

3.1 Introduction

Rising ambient temperatures and water scarcity entail adverse consequences on thermal power generation. The U.S. Geological Survey of 2010 estimated that thermoelectric power generation accounted to 38% of total freshwater consumption [1]. Thermoelectric plants that use water evaporation during cooling generated approximately 89% of the power in the United States in 1998 [2]. These rates of consumption entail a challenge to the field of thermoelectric power generation due to other competing uses for water such as domestic, industrial and agricultural. The location of many power plants allows the use of the water of a sea, a river, or a lake for cooling. However, federal regulations now prohibit new power plants from using water reservoirs for cooling due to ecological considerations. The only remaining option is the use of air as a sole coolant and/or cooling technologies with low water consumption.

An essential part of a thermal power plant that is mostly impacted by rising ambient temperatures and water scarcity is the condenser. This is because plant thermal efficiency increases at lower pressure and lower temperature condensation. However, as the ambient temperature increases, the temperature difference between the condenser surface and the atmosphere decreases. In an air-cooled condenser (ACC), the decrease in temperature difference

decreases the heat rejection capacity of the condenser considerably and decreases the thermal efficiency of the plant. Rising ambient temperatures caused incidents of shutdowns at power plants in the summers of 2011 and 2012 [3]. ACCs provide large surface area for heat transfer but correspond to relatively low heat transfer coefficients. Moreover, performance is limited by maldistribution of the air flow through the tube bundles [4], fin efficiency, and non-symmetric temperature fields. Cooling towers are used in conditions where the access to water reservoir are either impossible, limited, or prohibited by the law. Cooling towers are practical for heat rejection at higher ambient temperatures by mean of evaporation especially for landlocked arid locations. However, they use large quantities of water to make-up for evaporation in warmer climates [5] and require regular water recycling to limit the build-up of impurities.

Bustamante et. al. [6] modeled the performance of ACC's, reporting that a 68% increase in air-to-steam flow rate ratio reduced air-side thermal resistance by 66%. However, the improvement in thermal performance was negated by the increased pressure drop and fan power. Air jet impingement was mentioned as a possibility for ACCs because the enhanced heat transfer , but he usual fan power requirements were too high. They proposed using a cooling tower with an ACC during high ambient temperatures to conserve water. This idea can be implemented by either operating the ACC and the cooling tower as two separate units, or by the incorporation of an ACC section inside the cooling tower [7].

Another option is to use evaporation techniques with ACCs such as cooling the inlet air-side with direct sprays [8] or passing the air through wet towers. In both arrangements, upstream air cools and approaches wet-bulb temperature before it exchanges heat with steam. Evaporation cooling can also be conducted by deluging the air-side surface with water [9]. Latent and sensible heat is rejected through this technique. Spraying and deluging evaporation techniques showed

major enhancement on the thermal performance when incorporated with ACCs. However, a number of disadvantages are associated with these techniques. Incomplete evaporation of the spray droplets is an issue that can decrease thermal performance [10]. The unevaporated droplets attached to the air-side surface of the condenser downstream and caused severe corrosion with continuous operation [11]. Droplets size is considered in a number of studies [12,13] to determine the rate of droplet evaporation in sprays. Severe corrosion is also shown to be a major issue in the deluging approach [14]. Air-side surface coating and the use of higher water quality are suggested to mitigate corrosion [15]. Also, deluging causes increased pressure drop with increased flooding rates [16].

A number of studies explored new ideas for totally dry air-cooled condensers. A flapping vortex generator in a rectangular finned channel was numerically studied by Li et. al. [17]. The vortex generators are proposed to be mounted on an ACC air-side surface to enhance performance through introducing flow vortices. They reported a 140% enhancement in heat transfer due to attaching a Young's Modulus of 1 MPa vortex generator to a heat sink fin. Benn et. al. [18] conducted an analytical study to evaluate the use of thermosyphons in steam condensers. The thermal performance of two condenser designs that use thermosyphons was evaluated individually and in combination with a conventional cooling tower. The phase change process in thermosyphons provided higher capacities for heat rejection. High coefficients of performance were analytically reported. However, the performance of the thermosyphons can be compromised due to high ambient temperature as it is in the case of ACCs. Yousef et. al. [19] studied refrigerants as alternatives for steam condensation due to their low evaporation temperatures. They found that R-410 refrigerant performed superiorly, as compared to other refrigerants, in terms higher exergy

efficiency and energy rate. However, an analysis of the refrigeration cycle energy consumption and its impact on the overall thermal efficiency of the plant was not reported.

Microchannels cooling, and jet impingement are used to remove high rates of heat fluxes from electronics devices [20] and could be used for condensers, but rarely have in the past. Microchannel cooling has size limitations and is preferred for applications sizes of 0.07m by 0.07m or less as reported Lee and Vafai [21]. Jet impingement has been applied to a wide range of applications where high rates of heat and/or mass transfer are desired, especially for drying [22].

The current study represents a new approach of using hybrid dry/wet jet impingement cooling on the condensers of thermal power plants. We propose an array of air jets impinging on the air-side of a grooved plate condenser surface with the grooves containing water. The proposed approached is extremely rare on the literature. One study that demonstrate the potential of combining jet impingement with evaporation was conducted by Narayanan et. al. [23]. They studied heat and mass transfer of a jet impinging on a nanoporous membrane containing a film of water for electronic cooling. The study demonstrated the possibility of achieving high levels of heat flux at low jet speeds and water flow rates. The aim of the current study is evaluating the feasibility of a hybrid jet impingement by quantifying heat transfer and associated energy and water consumptions. A hybrid wet/dry jet impingement condenser would provide efficient dry and evaporative cooling in a single easy to operate unit.

3.2 Experimental Model

An array of jets at temperature T_o impinge on a grooved aluminum plate with water in the grooves is shown in figure 3.1. Water is contained in the grooves by means of gravity and the lateral heat transfer is restricted by insulation. The plate is maintained at constant temperature $T_s > T_o$ using a heater suppling power at a rate of q_T. The heat is transferred from the top surface at

steady state conditions by means of convection, evaporation and radiation. Transfer mechanisms are occurring simultaneously on the dry and wet portions of the surface as denoted on the figure. The corresponding energy balance of the arrangement shown in figure 3.1 is:

$$q_T = q_{conv,d} + q_{rad,d} + q_{conv,w} + q_{rad,d} + q_{Evap} \quad (1)$$

Where,

$$q_{conv,d} = h \cdot A_d \cdot (T_s - T_o) \quad (2)$$

$$q_{conv,w} = h \cdot A_w \cdot (T_w - T_o) \quad (3)$$

$$q_{rad,d} = \varepsilon_d \cdot \sigma \cdot A_d \cdot (T_s^4 - T_o^4) \quad (4)$$

$$q_{rad,w} = \varepsilon_w \cdot \sigma \cdot A_w \cdot (T_w^4 - T_o^4) \quad (5)$$

$$q_{Evap} = h_m \cdot A_w \cdot i_{fg} \cdot (C_w - C_o) \quad (6)$$

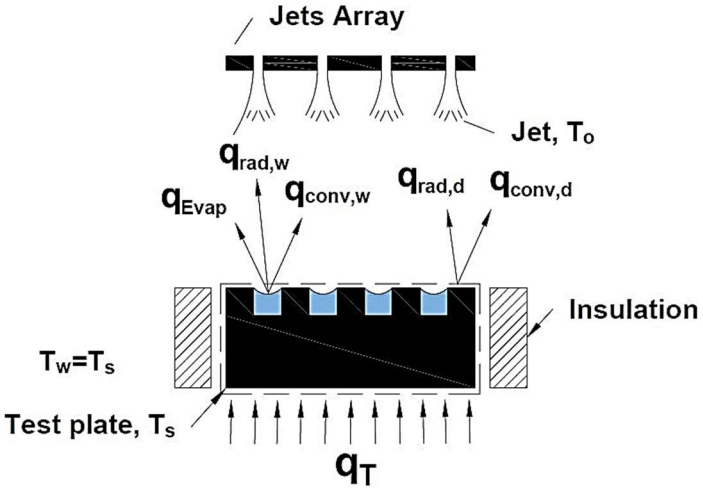

Figure 3. 1*: Energy balance and heat transfer mechanisms in hybrid jet impingement cooling.*

Where A_d and A_w are the dry and wet surface areas, respectively, normal to the direction of heat transfer. Also, h, h_m and i_{fg} are the convective coefficients of heat, mass transfer and the latent heat of vaporization of water, respectively. The emissivity of the dry and wet surfaces are denoted by ε_d, and ε_w, respectively. σ is Stefan-Boltzmann constant. C_w and C_o are the concentrations of

water in the air at the surface and at the jet opening, respectively. Both can be calculated, assuming equilibrium at the surface [24], as:

$$C_w = \left(\frac{1}{v_g}\right)_{@\ T_w} \tag{7}$$

And

$$C_o = \left(\frac{\emptyset}{v_g}\right)_{@\ T_o} \tag{8}$$

Where the Greek letter $\emptyset$ denotes the relative humidity.

Equation 1 can be simplified by number of assumptions such as: 1) Neglect radiation for low surface temperatures T_s, 2) assume T_w=T_s, 3) neglect wet surface curvature, and 3) use geometry of A_d=A_w. Applying these assumptions to equation 1 results in:

$$q_T = h \cdot A_t \cdot (T_s - T_o) + h_m \cdot A_w \cdot i_{fg} \cdot (C_s - C_o) \tag{9}$$

And

$$q_T/A_t = h \cdot (T_s - T_o) + h_m \cdot \frac{A_w}{A_t} \cdot i_{fg} \cdot (C_s - C_o) \tag{10}$$

Where A_t is the summation of A_d and A_w. Note that radiation should be considered for higher surface temperatures. It can be neglected at low surface temperatures T_s < 100ºC due to the small portion of 2% to 3% of heat transfer it accounts for at high convection and evaporation rates.

The mass transfer analogy [25] for a simultaneous heat and mass transfer process can be used to relate the heat and mass transfer coefficients and further simplify equation 10. The analogy is applicable for temperatures not near the boiling temperature of the liquid, low gas-to-evaporation flow rate ratios, and without dry out of the surface [26]. The convection heat and mass transfer coefficients can be related as:

$$\frac{h}{h_m} = \frac{k}{D_{AB} \cdot Le^n} \tag{11}$$

Where D_{AB} is the mass diffusivity coefficient, Le is the Lewis number, and k is the thermal conductivity of the air. Lewis number for a water-air mixture is given by:

$$Le = \frac{\alpha}{D_{w-a}} \tag{12}$$

Where α is the thermal diffusivity of air. For the current range of temperatures, the value of $Le^{2/3} = 0.9$, and n = 1/3 for most applications [28]. Thus, the mass transfer coefficient can be calculated as:

$$h_m = h\left(\frac{D_{w-a}}{k} \cdot Le^{1/3}\right) \tag{13}$$

Substituting for h_m in equation 10 gives:

$$q_T/A_t = h\left[(T_s - T_o) + \left(\frac{D_{w-a}}{k} \cdot Le^{1/3}\right) \cdot \frac{A_w}{A_t} \cdot i_{fg} \cdot (C_s - C_o)\right] \tag{14}$$

From which the convection heat transfer coefficient is calculated:

$$h = \frac{q_T/A_t}{\left[(T_s - T_o) + \left(\frac{D_{w-a}}{k} \cdot Le^{1/3}\right) \cdot \frac{A_w}{A_t} \cdot i_{fg} \cdot (C_s - C_o)\right]} \tag{15}$$

Water flow rate due to evaporation is calculated as:

$$\dot{m}_{Evap} = h \cdot \left(\frac{D_{w-a}}{k} \cdot Le^{1/3}\right) \cdot A_w \cdot (C_s - C_o) \tag{16}$$

Note that heat transfer in equation 14 can be achieved through evaporation even at high ambient temperature of T_s=T_o at $\emptyset$ < 100%. Moreover, evaporation can still take place at $\emptyset$ = 100% at T_s > T_o due to difference in concentrations of water ($C_s > C_o$) as described by equations 7 and 8. The energy that is required for evaporation will be absorbed solely from the surface instead of the air as is the case in cooling towers. Such capability and flexibility encourage the application of the proposed approach in the condensers of thermal power plant for a single high capacity hybrid condensing unit.

The coefficient of performance CP can be used to evaluate the efficiency of the proposed approached. CP is defined as the ratio of q_T to fan power P_f as:

$$CP = \frac{q_T}{P_f} \tag{17}$$

Where

$$P_f = \frac{\dot{\forall} \cdot \Delta p}{\eta_f} \tag{18}$$

Where $\dot{\forall}, \Delta p$, and η_f are the air volumetric flow rate, pressure difference, and fan efficiency, respectively. Fan efficiency is assigned a conservative value of 65%.

3.3 Experimental Setup

3.3.1 Apparatus

The experimental apparatus for measuring the average surface heat transfer coefficient is depicted in figure 3.2. A wind tunnel was used to supply air for the experiment at varying jet speeds by regulating the power supplied to an axial flow fan. A manometer was used to measure the static pressure in a vicinity of the orifice opening inside the plenum, though not shown in the figure. The appropriate Δp was maintained to satisfy the required jet speed as described by the Bernoulli equation:

$$U_o = \sqrt{\frac{2\Delta p}{\rho}} \tag{19}$$

A pitot tube was used to measure the jet velocity for a random sample of jets at each orifices plate to insure uniform exist velocity.

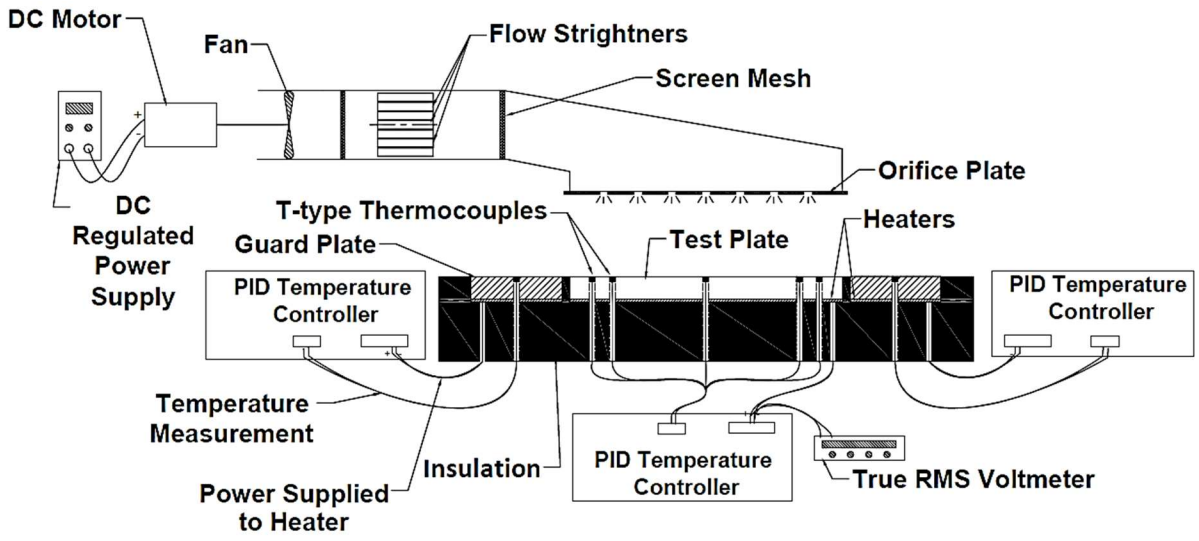

Figure 3. 2*: Abstract depiction of the experiment apparatus.*

Grooved test plates were mounted on an electric heater as depicted in figure 3.2. Rectangular grooves were milled into the surface of the 152.4mm by 152.4mm aluminum plates with dimensions as shown in figure 3.3. Water does not usually wet a surface uniformly. Therefore, the groove dimensions were chosen to ensure complete wetting of the surface. Levich [29] introduced an equation to calculate a capillary constant:

$$\lambda = \sqrt{\frac{\zeta}{\rho \cdot g}} \tag{20}$$

Where λ represents the characteristic length scale of the surface tension effects and ζ is the surface tension of water. The typical value for water is a little less than 3 mm. Consequently, groove widths of 3.56mm and 2.55mm were used and resulted in even wetting based on visual observation. The majority of experiments were performed with plate (b) in which each groove has a width and a depth of 3.56mm and a length of 147.3mm. The geometry results in a total of 21 equally spaced grooves one of which is aligned transversely and used as a water supply groove as shown in figure 3.4.

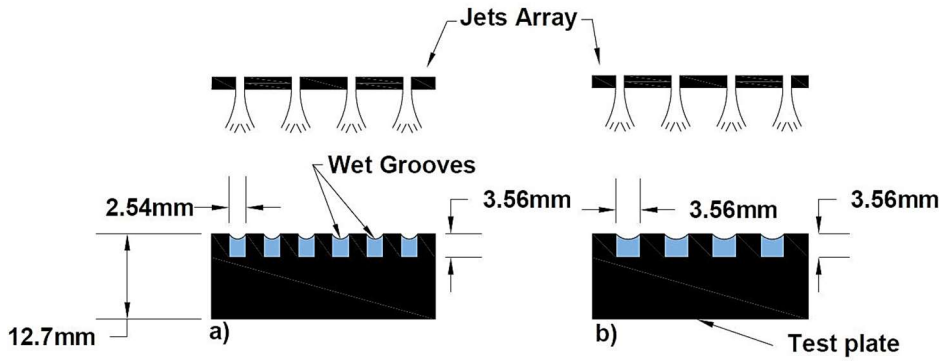

Figure 3. 3: *Test plates: a) Width=2.54mm and depth=3.556, b) Width and depth=3.556mm.*

Water covers 50% of the surface in plate (b) where A_w/A_t=0.5. Plate (a) has grooves that have the same depth and length as the plate (b) but a narrower width of 2.54mm. This geometry resulted in 30 grooves with A_w/A_t=0.5 for plate (a).

Figure 3.4 shows a top view of test plate (b) where 14 T-type thermocouples were distributed and press fit into the plate surface in different locations. A number of the thermocouples were fit into the bottom of the grooves while some thermocouples were fit into the dry portion of the plate as shown. The distribution of the thermocouples in such manner is to ensure the uniformity of temperature measurement. Eight of the thermocouples were wired in parallel and supplied to a Eurotherm 810 PID temperature controller. The controller was used with a Eurotherm 831 Silicon Control Rectifier (SCR) to supply power to the heater. Therefore, it is necessary to use a true-RMS voltmeter (HP-3486A) to measure the voltage to determine the power supplied to the heater. Once voltage V was measured, the power was calculated as:

$$\mathcal{P} = \frac{V^2}{\mathcal{R}} \tag{21}$$

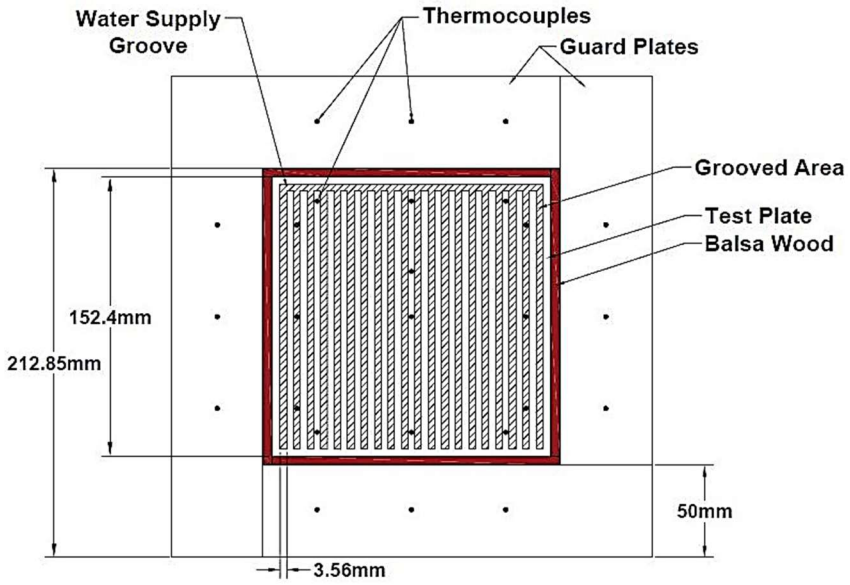

Figure 3. 4*: Top view of test Plates b with guard plates and thermocouples locations.*

Where $\mathcal{R}$ is the electrical resistance of the heater. Temperature readings from the remaining six thermocouples were recorded individually using an NI-9214 DAQ system. To minimize edge losses, four guard plates surrounded the test plate and were maintained at the same set-point temperature as the test plate using additional PID controllers and SCR's. The test plate and the guard plates were placed on a multilayer of insulation materials of wood and fiberglass to minimize the conduction losses.

In performing the experiment, heated water is introduced to the transverse water supply groove which then flows to the remaining grooves. This is done to ensure minimal fluctuation of the surface temperature, while experimenting.

Six different jet arrays were made by drilling circular holes in 1.6 mm (1/16") aluminum plates. The open area A_o is the ratio between the area of the orifices and the test plate surface area. The additional side surface area of the grooves are not included and A_o is calculated as:

$$A_o = \frac{C_D \cdot N \cdot \frac{\pi}{4} d^2}{A_s} \tag{22}$$

Where N is the total number of jets in the array and C_D is the discharge coefficient.

As shown in figure 3.5, three of the arrays, a to c, have the same value of the open area A_o =1.5% but at different orifice diameters of 3.18mm, 4.76mm, and 6.35mm. The diameter of orifices in the remaining arrays, d to f, was fixed at 4.76mm while the value of A_o was varied with values of 1%, 2%, and 3%.

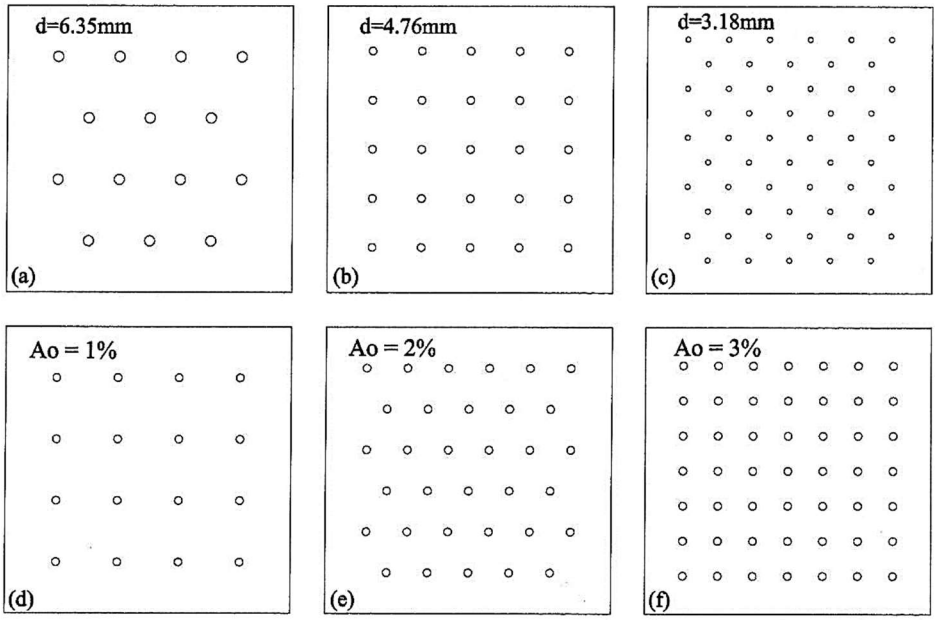

Figure 3. 5: *Jets array: (a) to (c), A_o=1.5% with different diameters, (d) to (f), d=4.76mm with variable A_o.*

The number of orifices and the configuration in each array is given by:

$$N = \frac{A_O \cdot A_S}{C_D \cdot \frac{\pi}{4} \cdot {d_e}^2} \tag{23}$$

The arrays were fabricated in a CNC mill to ensure that all orifices in each plate have the same geometrical characteristics.

Most jet arrays are produced using orifices in thin plates with discharge coefficients of C_D between 0.75 to 0.85, because of the contraction of the flow as it turns through the orifice. This gives an effective diameter of:

$$d_e = d\sqrt{C_D} \tag{24}$$

Although shown to be important to the resulting heat transfer [30], many jet array studies overlook this effect. To measure C_D, water flow was used for a sample of n orifices in each array. The Reynolds number based on the orifice diameter Re_d was used to match air and water velocities. Reynolds number ranged from 4,070 to 12,210. The corresponding water head was maintained at a prescribed level by regulating water flow to the container with the orifice plate beneath it. Water was allowed to flow through the selected orifice and the flow rate of water $\dot{m}_w$ was measured using an electronic weight scale and a timer. The discharge coefficient then was calculated as:

$$C_D = \frac{\dot{m}_w}{\rho_w \cdot \frac{\pi}{4} \cdot d^2 \cdot {U_{o,w}}^2} \tag{25}$$

Table 1 shows the measured discharge coefficients for the three different orifice sizes and resulting effective diameter. Cd was observed to be independent of Re_d.

Table 3. 1: *Discharge coefficients, CD*

d(mm)	# of experiments	C_D	C_D standard deviation	de(mm)
3.18	6	0.784	0.003	2.81
4.76	6	0.785	0.005	4.22
6.35	6	0.802	0.002	5.69

3.3.2 Procedure and Data Reduction

When gas jets strike liquid surfaces they have been shown to cause the liquid to deform, dimple, and splash [30]. Moreover, droplets can escape the liquid surface due to horizontal and vertical liquid oscillations, liquid shearing due to gas stream, entrainment of liquid into the gas jet, and liquid surface ripples [32,33]. The gas jets were also shown to induce vortices within the liquid and detailed structures of such vortices have been numerically and experimentally reported. Therefore, the maximum jet speed and minimum stand-of distance at which splashing of water in

the grooves occurs was experimentally observed and avoided. A majority of the experiments were performed on test plate (b) in figure 3.2. For each jet array in figure 3.5, jet velocities U_o of 5m/s, 7.5m/s, and 10m/s, were used. At each U_o, three stand-off distance ratios H/d_e of 5.4, 7.18, and 12 were used. Experiments were performed, for the mentioned test variables, at two surface temperatures T_s of 25°C (ambient) and 42.8°C. Relative humidity $\emptyset$ was not controlled, but was recorded using WT Meter - Digital Psychrometer. Nine experiments were performed on test plate (a) to explore the effect of grooves width on heat transfer. The resulting total number of experiments performed was 117.

Average heat transfer coefficients were obtained through the measurement of power supplied to the heater under a given T_s, A_o, U_o and H/d_e ratio. The power was controlled to sustain the surface temperature T_s of the test plate. The system required an average of 45 minutes to reach steady state. A temperature standard deviation of 1.5°C in T_s, between the six thermocouples mounted in the plate was observed. At the steady state condition, surface temperature T_s, air temperature T_o, relative humidity $\emptyset$, voltage V, and electrical resistance $\mathcal{R}$ were logged. The electrical power $\mathcal{P}$ supplied to the heater was calculated using equation 21. The resulting heat flux was calculated as:

$$q^{"} = \mathcal{P}/A_t \tag{26}$$

Note that q" can be equated to q_T/A_t in equation 10. Therefore, the average convection heat transfer coefficient was calculated as:

$$h = \frac{q^{"}}{\left[(T_s - T_o) + \left(\frac{D_{w-a}}{k}.Le^{1/3}\right).\frac{A_w}{A_t}.i_{fg}.(C_s - C_o)\right]} \tag{27}$$

Where the values of D_{w-a}, k, Le, C_w, and C_o were calculated based on the measured T_s and T_o. The average Nusselt number based on the effective jet diameter d_e is:

$$Nu = \frac{h \cdot d_e}{k} \tag{28}$$

The above-mentioned procedure was repeated 36 times and performed for each reported measurement.

The conduction heat losses q''_{cond} were divided into lateral loss and downward loss. The lateral loss was significantly diminished due to the use of four guard plates surrounding the test plate and the loss was neglected. The downward loss was estimated as less than 1% of the power dissipated by the heater. This estimation was obtained through thermal resistance analysis for the upward and downward mediums enclosing the heater. The radiation losses were divided into losses from the dry portion of the test plate and the wet portion of the plate. For A_d=A_w, the radiative heat loss per unit area, neglecting radiation from the side surfaces of the grooves, is calculated as:

$$q''_{rad} = \sigma \cdot [\varepsilon_d \cdot (T_s^4 - T_o^4) + \varepsilon_w \cdot (T_w^4 - T_o^4)] \tag{29}$$

The water emissivity ε_w was estimated to be 0.96 [36]. The dry surface emissivity ε_d value was found to be 0.76. This estimation was obtained by using FLIR SC600 Series High-Resolution LWIR Science-Grade infrared camera where a portion of the test plate was painted with a black paint with a known value of ε_b= 0.94, while another portion remained unpainted. The infrared picture of the plate indicated the different temperatures for the painted and unpainted portions of the plate. Accordingly, the emissivity of the plate was obtained as:

$$\varepsilon_d = \frac{T^4_{unpainted}}{T^4_b} \cdot \varepsilon_b \tag{30}$$

The percentage of heat transfer due to radiation was found to vary from 1.1% to 3.6% of $\mathcal{P}/A_t$ depending on the magnitude of the convection and evaporation portions of heat transfer.

3.3.3 Data Statistics and Uncertainty

Confidence intervals were constructed for the measured values of Nu. For each test, 36 values of Nu were recorded to give the mean value, standard deviation, and the 95% confidence

interval. It was observed that the size of the confidence interval varied between 6% to 7% of the estimated mean value of Nu.

The sources of uncertainty in the measurement of Nu are listed in table. 2 with the respective uncertainty values. Parameters were selected based on the expression that was adopted to calculate Nu such as:

$$Nu = \frac{h\, d_e}{k} = \frac{V^2/\mathcal{R}}{\left[(T_s - T_o) + \left(\frac{D_{w-a}}{k} Le^{1/3}\right) \cdot \frac{A_w}{A_t} i_{fg} \cdot (C_s - C_o)\right]} \cdot \frac{d_e}{k \cdot A_t} \tag{31}$$

Therefore, the uncertainty on Nu was estimated as:

$$U_{n_{(Nu)}} = \left\{ \left[\frac{\partial}{\partial V}(Nu) \cdot U_{n_V}\right]^2 + \left[\frac{\partial}{\partial \mathcal{R}}(Nu) \cdot U_{n_{\mathcal{R}}}\right]^2 + \left[\frac{\partial}{\partial d_e}(Nu) \cdot U_{n_{d_e}}\right]^2 + \left[\frac{\partial}{\partial T}(Nu) \cdot U_{n_T}\right]^2 + \left[\frac{\partial}{\partial A_t}(Nu) \cdot U_{n_{A_t}}\right]^2 + \left[\frac{\partial}{\partial A_w}(Nu) \cdot U_{n_{A_w}}\right]^2 + \left[\frac{\partial}{\partial k}(Nu) \cdot U_{n_k}\right]^2 + \left[\frac{\partial}{\partial (D_{w-a})}(Nu) \cdot U_{n_{(D_{w-a})}}\right]^2 + \left[\frac{\partial}{\partial (i_{fg})}(Nu) \cdot U_{n_{(i_{fg})}}\right]^2 + \left[\frac{\partial}{\partial (C_s)}(Nu) \cdot U_{n_{C_s}}\right]^2 + \left[\frac{\partial}{\partial (C_o)}(Nu) \cdot U_{n_{C_o}}\right]^2 \right\}^{\frac{1}{2}} \tag{32}$$

Note the dependence on temperature of the uncertainties of D_{w-a}, k, C_s, and C_o. The dominant uncertainty source is thus the temperature. The resulting value of uncertainty in Nu was found to be 8%-10%.

The confidence interval value of the data and the estimated uncertainty of the Nu are both indicators of the quality of the experiment and of the results produced.

Table 3. 2*: Uncertainty sources for the wet grooved surface.*

#	Source of uncertainty	Value	Unit
1	Voltage measurement, U_{n_V}	0.02% of measured V	volt
2	Resistance measurement, $U_{n_{\mathcal{R}}}$	0.5% of measured $\mathcal{R}$	ohm
3	Temperature measurement, U_{n_T}	1.5	K
4	Surface area measurement, $U_{n_{A_{w,t}}}$	3.4×10^{-4}	m^2
5	Thermal conductivity value, U_{n_k}	1.3×10^{-4}	W/(m-K)
6	Orifice diameter measurement, $U_{n_{d_e}}$	4×10^{-5}	m
7	Mass diffusivity uncertainty, $U_{n_{(D_{w-a})}}$	0.04×10^{-5}	m^2/s
8	Water concentration at the surface $U_{n_{C_s}}$	7.33×10^{-7}	kg/m^3
9	Water concentration in jet air $U_{n_{C_o}}$	5.06×10^{-7}	kg/m^3

10	Water latent heat uncertainty $U_{n_{(i_{fg})}}$	5.6	kJ/kg

3.4 Results and Discussion

For a prescribed U_o, A_o, and H/d_e, experiments were performed at two surface temperatures T_s=42.8ºC and T_s=T_o. At T_s=T_o, heat transfer occurs solely due to evaporation since convection is zero and, thus,

$$q_{Evap} = \mathcal{P} \tag{33}$$

And accordingly, convection mass transfer coefficient is simply:

$$h_m = \frac{\mathcal{P}}{A_w \cdot i_{fg} \cdot (C_w - C_o)} \tag{34}$$

The mass transfer coefficient was used to calculate the evaporation rate and to obtain the respective heat transfer coefficient using equation 13. For T_s=42.8ºC, the convection heat transfer coefficient and respective Nu are obtained using equation 27 and 28, respectively. The results are then compared to convection heat transfer coefficients and Nusselt numbers that were obtained at T_s=T_o and similar U_o, A_o, and H/d_e. Moreover, Nu numbers will be compared to Nu numbers of jet impingement on dry grooves at T_s=42.8ºC (part-I of the study). The purpose of this comparison is to test the validity of the heat and mass transfer analogy under different operating conditions.

Figures 3.6 to 3.9 show the variation of average Nu against H/d_e for jet arrays (a), and (c) (as shown in figure 3.5). The A_o for the arrays is 1.5%, however, d_e is 5.69mm for array (a), and 2.81mm for array (c). Reynolds number Re_{de} for U_o values of 5m/s and 10m/s is shown in the figure. Nusselt number results are presented for experiments of wet surface at T_s=T_o, wet surface at T_s= 42.8ºC and dry grooves at T_s=42.8ºC. Experimental uncertainty is represented by bars plotted on each measurement. The number of jets increases as d_e decreases for a fixed A_o. the figures show that the Lewis relation, equation 13, provided reasonable prediction accuracy for h

from of the knowledge of h_m or vice versa. Results of Nu, obtained at wet and dry surfaces, fall within the uncertainty limits under for the denoted test conditions. The prediction accuracy is improved for lower jet speeds U_o and lower diameters d_e. Nu results showed usual trends of jet impingement even when evaporation is involved. Nu decreased with increasing H/d_e ratio and increased with increasing Re_{de}. Such observations make the proposed approach robust and simple in prediction of a hybrid dry/wet heat transfer process. The latter does not apply to other hybrid cooling techniques such spray and mist cooling in which heat transfer modes are extremely complex and interdependent as reported by Cheng et. al. [37].

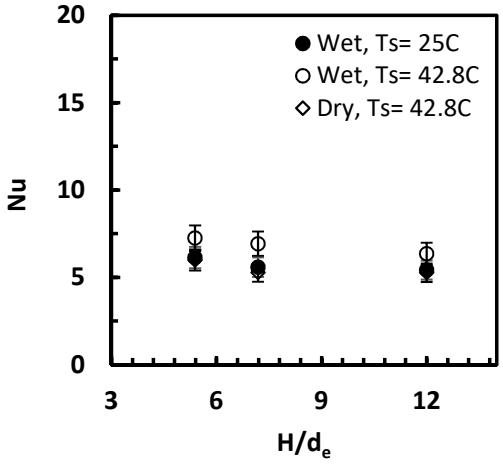

Figure 3. 6*: Nu vs H/de for de=2.81mm, A_o=1.5%, U_o=5m/s, and Re_{de}=889.*

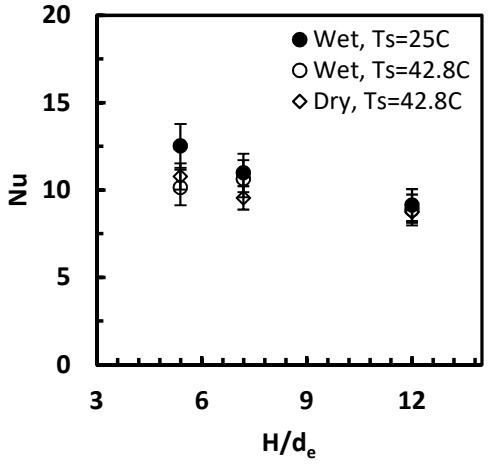

Figure 3. 7*: Nu vs H/de for de=5.69mm, A_o=1.5%, U_o=5m/s, and Re_{de}=1,780.*

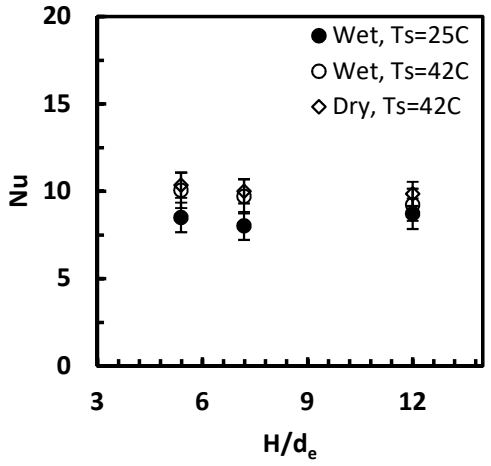

Figure 3. 8: *Nu vs H/de for de=2.81mm, A_o=1.5%, U_o=10m/s, and Re_{de}=1,780.*

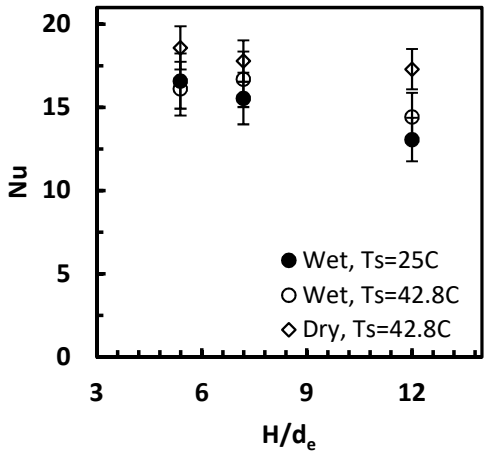

Figure 3. 9: *Nu vs H/de for de=5.69mm, A_o=1.5%, U_o=10m/s Re_{de}=3,560.*

Figures 3.10 to 3.13 show the variation of the average Nu with H/d_e for jet arrays (d), and (f) (as shown in figure 3.5). The diameter d_e is 2.81mm for all the arrays, however, A_o is 1% for array (d), and 3% for (f). The Re_{de} for jet speeds 5m/s and 10m/s is shown in the figure. Nusselt number results are presented for experiments of wet surface at $T_s=T_o$, wet surface at T_s= 42.8ºC and dry at T_s=42.8ºC. Experiment uncertainty is represented by bars plotted on each measurement. Number of jets increase as A_o increases for a fixed d_e. The prediction accuracy of the mass transfer analogy is shown to increase for lower A_o percentages and lower U_o. However, all results are within the uncertainty limits of the experiments excepts for figure 3.13. The figures show Nu to increase as A_o, and U_o increase as expected in jet impingement cooling.

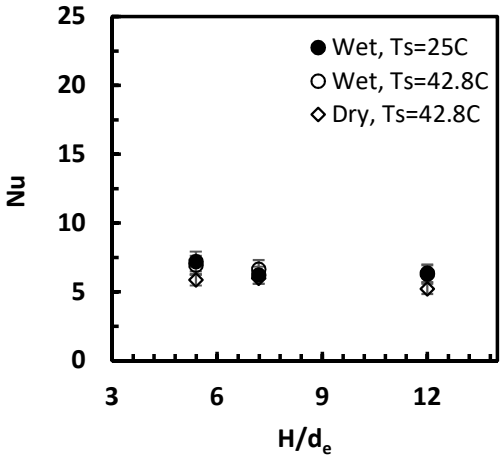

Figure 3. 10: *Nu vs H/de for de=4.22mm, A_o=1%, U_o=5m/s, and Re_{de}= 1,335.*

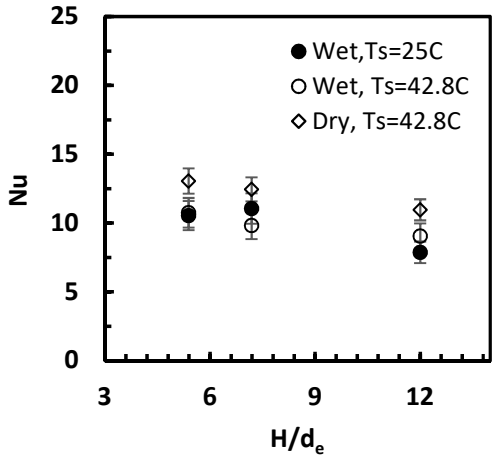

Figure 3. 11: *Nu vs H/de for de=4.22mm, A_o=3%, U_o=5m/s, and Re_{de}= 1,335..*

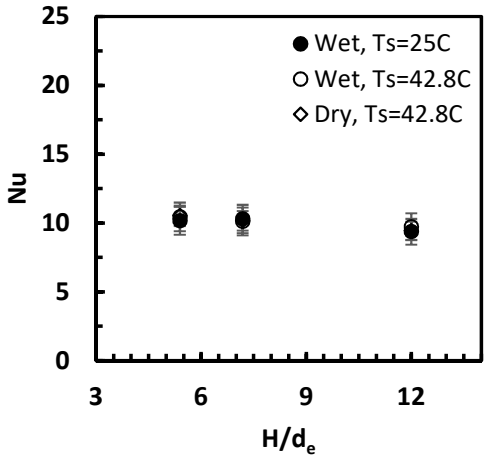

Figure 3. 12: *Nu vs H/de for de=4.22mm, A_o=1%, U_o=10m/s, and Re_{de}= 2,670.*

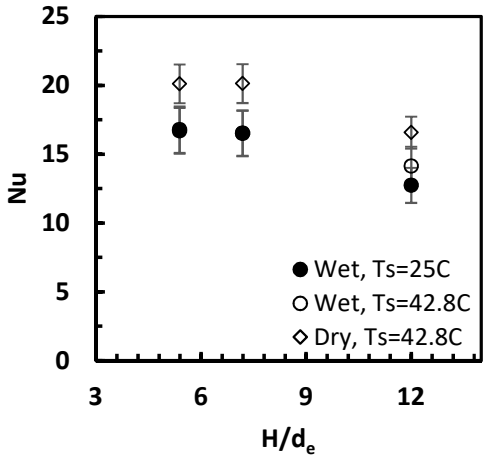

Figure 3. 13: *Nu vs H/de for de=4.22mm, A_o=3%, U_o=10m/s, and Re_{de}= 2,670..*

The relative humidity Ø in the room was not controlled and varied from one day to another. Consequently, experimentally measured heat transfer coefficients were used to analytically calculate q_T/A_t at a Ø = 50%, T_s=45°C, and T_o=25°C as given by equation 14. The resulting heat fluxes values are compared in figures 3.14 to 3.15. The A_o for the arrays is 1.5%, however, d_e is different as denoted. As shown in the figure 3.15, the highest achieved q" is 7,400W/m^2. Heat flux q" increased as d_e decreased from 5.69mm to 2.81mm at the same test conditions. It can be observed that at low U_o=5m/s, q" increased by 30%-44% when d_e decreased from 5.69mm to

2.81mm. However, at U_o=10m/s, q" increased by only 18%-29% when d_e decreased by half. This means that heat transfer is more efficient at smaller d_e and/or lower U_o. The latter mentioned trend was observed for jet impingement cooling of flat surfaces [38].

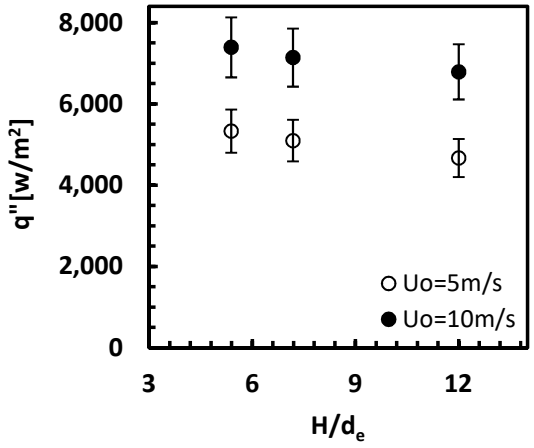

Figure 3. 14: *q" for hybrid impingement cooling at d=2.81mm, T_s=45°C, T_o=25°C, Ø=50%, and A_o=1.5%.*

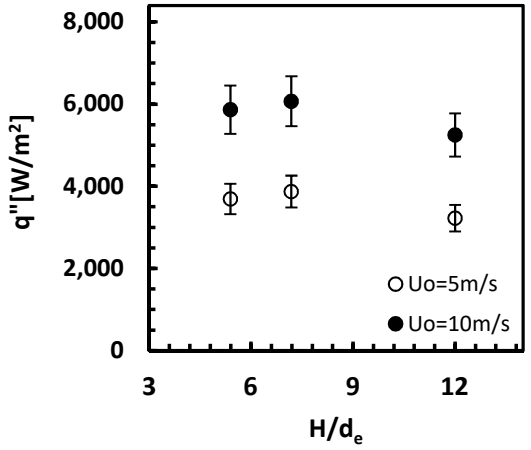

Figure 3. 15: *q" for hybrid impingement cooling at d=5.69mm, T_s=45°C, T_o=25°C, Ø=50% and A_o=1.5%.*

Figures 3.16 and 3.17 shows q" variation with open area A_o for hybrid wet/dry jet impingement cooling. Jet speeds U_o are 5m/s and 10m/s and d_e=4.76mm. As shown in the figure 3.17, highest achieved q" is 8,230W/m^2. Increased A_o value increases the air flow rate at constant speed linearly. q" increases as A_o increases at both jet speeds of 5m/s and 10m/s. It can be observed that at A_o=3%, q" increased by about 18% when H/d_e decreased from 12 to 5.4. However, at A_o=1%, heat flux only increased by about 8% as H/d_e decreased from 12 to 5.4. Also, at H/d_e=12, q" increased by 30%-42% as A_o tripled. This in comparison to 40%-55% increase in q" when A_o increased from 1% to 3% at H/d_e=5.4. From these observations it can be concluded that heat transfer is more receptive to changes in H/d_e at higher A_o percentages. Similar trends were observed for jet impingement cooling of flat surfaces [38].

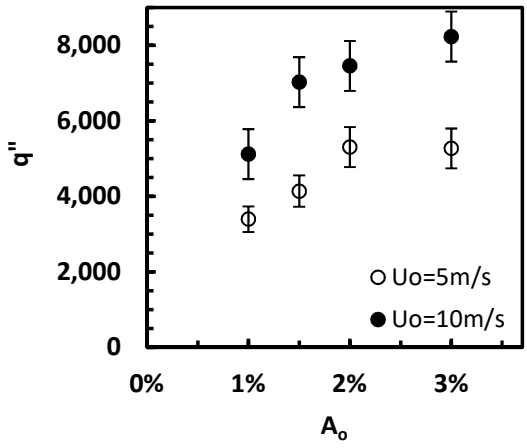

Figure 3. 16: *q" vs A_o for hybrid jet impingement cooling at d=2.81mm, T_s=45°C, T_o=25°C, Ø=50%, H/d_e=5.4, and d_e=4.22mm.*

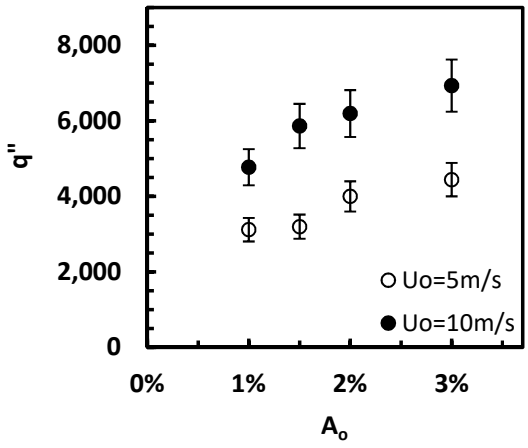

Figure 3. 17: *q" vs A_o for hybrid impingement cooling at d=2.81mm, T_s=45°C, T_o=25°C, Ø=50%, H/d_e=12, and d_e=4.22mm.*

Figures 3.18 to 3.21 show the improvement of heat transfer for two hybrid wet/dry jet impingement cooling obtained at two U_o values of 5m/s and 10m/s. q" for the hybrid regime is compared to q" of jet impingement cooling of a dry flat surface reported in [38]. Figures 3.18 and 3.19 show q" variation with H/d_e at A_o=1.5% for two d_e values as denoted. Figures 3.20 and 3.21, show q" variation with H/d_e at d_e=4.76mm and different A_o values. It can be observed that heat flux increases on a dry grooved surface is 15%-50% higher than q" of jet impingent a flat surface. Part-I of this study address in details jet impingement cooling of a dry grooved surface. The figures show that q" of jet impingement on a wet grooved surface increased by a remarkable 500% in comparison to flat surface q". The 500% increase was observed for all the test parameters that are denoted on the figures.

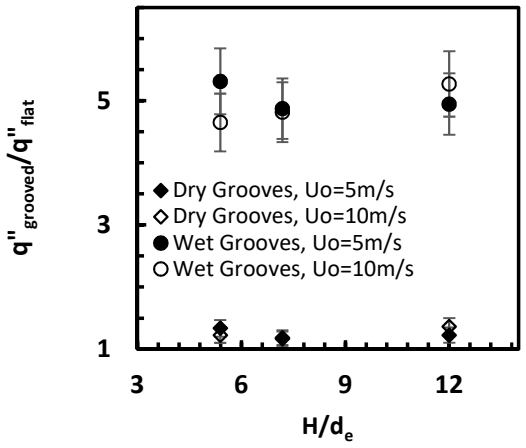

Figure 3. 18: *heat transfer improvement vs H/d_e for d_e=2.81mm, A_o=1.5%, and U_o=5m/s, 10m/s.*

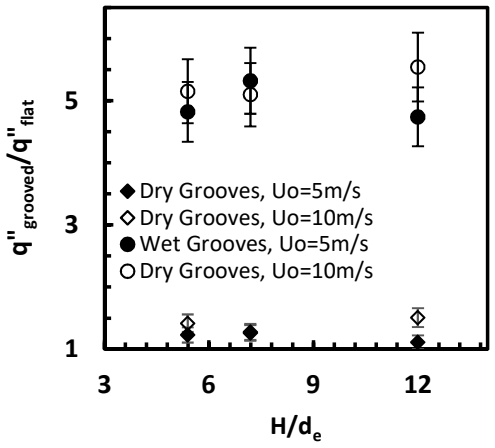

Figure 3. 19: *heat transfer improvement vs H/d_e for d_e=5.69mm, A_o=1.5%, and U_o=5m/s, 10m/s.*

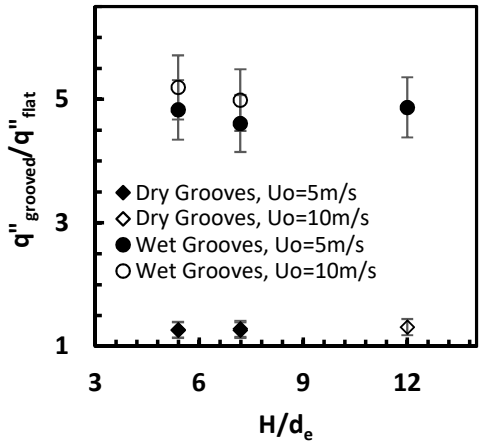

Figure 3. 20: *heat transfer improvement vs H/d_e for d_e=4.22mm, A_o=1%, and U_o=5m/s, and 10m/s.*

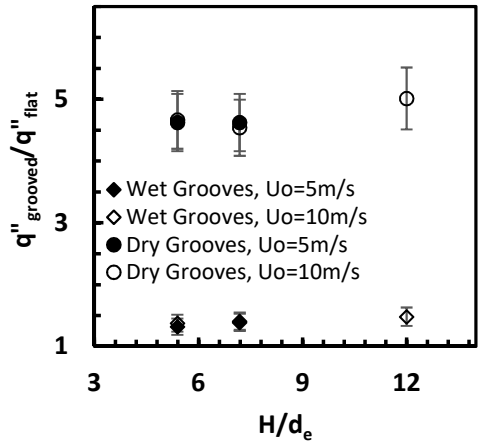

Figure 3. 21: *heat transfer improvement vs H/d_e for d_e=4.22mm, A_o=3%, and U_o=5m/s, and 10m/s.*

The coefficient of performance CP was used to evaluate the efficiency of hybrid jet impingement cooling. CP is the ratio of heat transfer to fan power as described by equation 17. Figures 3.22 and 3.23 show the CP values obtained at two U_o values of 5m/s and 10m/s, T_s=45ºC, T_o=25ºC, and 50% relative humidity. The highest Achieved CP value is 3,130 at d_e=2.81mm, U_o=5m/s, A_o=1.%, T_s=45ºC, T_o=25ºC and Ø=50%. For the same U_o, CP increased by 26%-30% when d_e decreased by half at H/d_e=5.4. This compares to a 44% increase in CP at the same U_o with H/d_e=12. A notable decrease of 80% in CP was observed when U_o increased from 5m/s to

10m/s at the same d_e and h/de ratio because of the huge increase in fan power. In [38], the CP values of jet impingement cooling of a flat surface where compared to CP values of ACCs and cooling towers. Jet impingement offered a significant 300% improvement in CP. In the current study, CP values for the hybrid jet impingement showed an average of 500% improvement when compared to jet impingement cooling of a dry flat surface. This means that the hybrid jet impingement cooling can achieve an improvement on CP of ACCs and of the magnitude of 1,500%. This is compared to improvements of 68% [6], 140% in [17], 700% in [15] and a maximum CP value of 423 in [18]. Consequently, hybrid jet impingement can provide an efficient high capacity alternative for steam condensers of thermoelectric power plants.

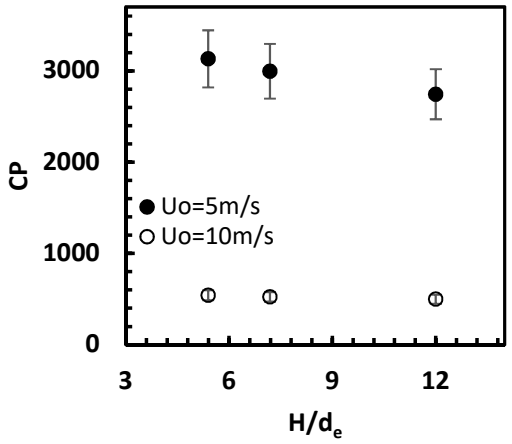

Figure 3. 22: *CP vs H/d_e for d_e=2.81mm, A_o=1.5%, and U_o=5m/s, 10m/s.*

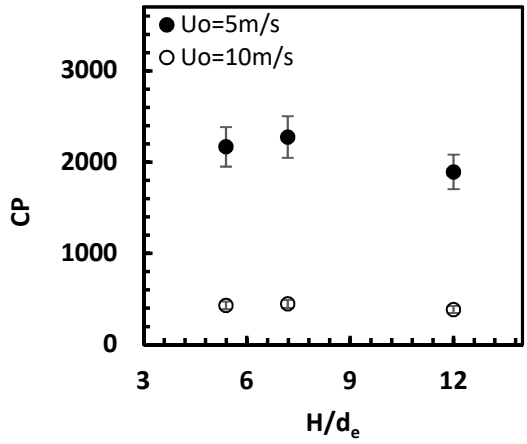

Figure 3. 23: *CP vs H/d_e for d_e=5.69mm, A_o=1.5%, and U_o=5m/s, 10m/s.*

Water consumption of wet cooling towers are presented and analyzed in [39] for power plants in different sites and different operation conditions. The study reported that water consumption for the cooling tower in a 500MW combined cycle plant ranges from 2,250 to 2,800 gallon/minute (gpm). For thermal efficiency of 51%, the condenser cooling load is 480.4MW. The consumption rates can be presented in terms of power generated as 4.5 to 5.6 gpm/MW. For hybrid jet impingement, water consumption for the case of highest CP=3,130 ratio will be

calculated in terms of gpm/MW, using equation 10, for jet speed U_o=5m/s, d_e=2.81mm, A_o=1.5%, H/d_e=5.4, T_s=45°C, T_o=25°C, and Ø=45%. the heat flux q"= 5,413W/m^2 and the required heat transfer area for 480.4MW load is 88,739.1m^2. Evaporation accounts for 81% of q" and the respective water consumption is 2,541.6gpm calculated using 17. This rate can be presented as 5.04 gpm/MW. This consumption rate is comparable to the consumption in cooling towers with high air flow rates and 330 < CP < 450 as reported in [39]. Because CP>3,000 for the hybrid jet impingement, hybrid jet impingement would require 80% less fan power. Evaporation can occur for T_s=T_o for Ø < 100% and, also, at Ø=100% for T_s>T_o due to the different water concentration between air and the concentration at the surface. In cooling towers evaporation is constrained by the wet-bulb temperature with spray techniques.

3.5 Conclusion

A new approach of hybrid jet impingement cooling was proposed as an alternative for steam condensers of thermoelectric power plants. Jets cooled a grooved surface at a constant temperature with the grooves containing water. The mass transfer analogy provided accurate predictions for the simultaneous process of heat and mass transfer. High magnitudes of heat flux were observed at low jet speeds and flow rates using hybrid jet impingement cooling. Similar heat transfer behavior to jet impingement on a flat surface was observed for hybrid jet impingement as q" changes with changing operation conditions. Heat transfer of hybrid jet impingement showed 500% improvement as compare to jet impingement on a flat surface. Hybrid jet impingement showed 600% to 1,500% improvement on the thermal performance as compared to air-cooled condensers and wet cooling towers. The proposed approach allows the efficient use of water since evaporation energy is absorbed from the steam and not used to cool air as in conventional evaporative cooling techniques. Hybrid jet impingement cooling is not constrained by the wet-

bulb temperature as it is the case for cooling towers, spray cooling, and mist cooling. The results encourage the application of hybrid jet impingement to the condensers of thermoelectric power plants and other related fields such as air-conditioning and refrigeration.

Nomenclatures

A	Area(m^2)
d	Diameter(m)
C	Water concentration(kg/m^3)
D_{AB}	Binary diffusion coefficients(m^2/s)
D_{w-a}	Water-air diffusion coefficients(m^2/s)
g	Gravitational acceleration(m/s^2)
h	Heat transfer Coefficient(m^2/s)
H	Orifice to surface distance(m)
h_m	Mass transfer Coefficient(m^2/s)
i_{fg}	Latent heat of evaporization(J/kg)
k	Thermal conductivity($W/m\text{-}\ ^oC$)
Le	Lewis number
$\dot{m}$	Mass flow rate(kg/s)
P_f	Fan power(W)
p	Pressure(Pa)
q	Heat transfer(W)
q_T	Total Heat transfer(W)
q"	Heat flux(W/m^2)
$\mathcal{R}$	Electrical resistance(ohm)
T	Temperature(^oC)
U	Velocity(m/s)
U_{n_A}	Uncertainty in surface area(m^2)
$U_{n_{C_o}}$	Uncertainty in water concentration in jet air(kg/m3)
$U_{n_{C_s}}$	Uncertainty in water concentration at the surface(kg/m3)
$U_{n_{d_e}}$	Uncertainty in diameter(m)
$U_{n_{(D_{w-a})}}$	Uncertainty in mass diffusivity coefficient(m2/s)
U_{n_k}	Uncertainty in thermal conductivity($W/m\text{-}\ ^oC$)
$U_{n_{\mathcal{R}}}$	Uncertainty in eelectrical resistance(ohm)
U_{n_T}	Uncertainty in temperature measurement(^oC)

U_{n_V}	Uncertainty in voltage (volts)
V	Voltage (volts)
$\dot{\forall}$	Air volumetric flow rate(m3/s), $\dot{\forall} = [A_s \cdot A_o] \cdot U_o$
υ	Kinematic viscosity(N/m^2)
v_g	Vapor specific volume(m^3/kg)
Δp	Pressure difference(Pa)
α	Thermal diffusivity(m^2/s)
ζ	Water surface tension(N/m)
ρ	Density(kg/m^3)
σ	Stefan-Boltzmann constant ($\sigma = 5.66961 \times 10^{-8}\ W/m^2 \cdot K^4$)

Non-dimensional

A_o	Open area percentage(%)
C_D	Discharge coefficient
CP	Coefficient of performance
ε	Emissivity
Le	Lewis number($\frac{\alpha}{D_{w-a}}$)
N	Number of Jets
Nu	Nusselt number ($h \cdot d_e/k$)
n	Power factor
$U_{n_{Le}}$	Uncertainty in Lewis number
$U_{n_{(Nu)}}$	Uncertainty in Nusselt number
Re_{de}	Reynolds number ($U_o \cdot d_e/\upsilon$)
η_f	Fan efficiency
∅	Relative humidity

Subscripts

b	Black body property
cond	Conduction
conv	Convection
d	Dry
e	Effective
Evap	Evaporation
Flat	
o	Jet exit property
rad	Radiation

s	Surface Property
t	Total
w	Water

References

[1] M.A. Maupin, J.F. Kenny, S.S. Hutson, J.K. Lovelace, Nancy L. Barber, K.S. Linsey, Estimated use of water in the United States in 2010: U.S. Geological Survey Circular 1405, (2014). https://dx.doi.org/10.3133/cir1405.

[2] Energy Information Administration, Annual Energy Review 1998, (1999).

[3] J. Rogers, K. Averyt, S. Clemmer, M. Davis, F. Flores-Lopez, P. Frumhoff, D. Kenney, J. Macknick, N. Madden, J. Meldrum, Water-smart power: Strengthening the US electricity system in a warming world, Camb. MA Union Concerned Sci. (2013).

[4] J. Wen, D. Tang, Z. Wang, J. Zhang, Y. Li, F. Sun, Numerical Simulation of Flow and Heat Transfer of a Direct Air-Cooled Condenser Cell in a Power Plant, in: American Society of Mechanical Engineers, 2013: p. V001T03A035-V001T03A035.

[5] N.P. Cheremisinoff, P.N. Cheremisinoff, Cooling towers selection, design and practice, Ann Arbor Science,Ann Arbor, MI, United States, 1981. https://www.osti.gov/servlets/purl/5913547.

[6] J.G. Bustamante, A.S. Rattner, S. Garimella, Achieving near-water-cooled power plant performance with air-cooled condensers, Appl. Therm. Eng. 105 (2016) 362–371. doi:10.1016/j.applthermaleng.2015.05.065.

[7] S. Taghian Dehaghani, H. Ahmadikia, Retrofit of a wet cooling tower in order to reduce water and fan power consumption using a wet/dry approach, Appl. Therm. Eng. 125 (2017) 1002–1014. doi:10.1016/j.applthermaleng.2017.07.069.

[8] J. Maulbetsch, M. DiFilippo, Spray enhancement of air cooled condensers, EPRI Palo Alto CA Calif. Energy Commision Sacram. CA Crockett Cogener. (2003).

[9] T. Conradie, D. Kröger, Enhanced performance of a dry dry-cooled power plant through air precooling, in: 1991.

[10] J.A. Heyns, Performance characteristics of an air-cooled steam condenser incorporating a hybrid (dry/wet) dephlegmator, (2008).

[11] M. Woest, I. Hearn, S. Lennon, Investigation Into The Corrosion Behaviour Of Galvanized Finned Tubing For Cooling Under Enhanced Wet/Dry Cooling Conditions, ESCOM, Scientific Investigations Report No. S91, 1991.

[12] G.P. Wachtell, Atomized Water Injection to improve dry cooling tower performance, Franklin Institute Research Labs, Philadelphia,(US), 1974.

[13] K. Duvenhage, Warmteruiling met adiabatiese voorverkoeling, (1993).

[14] M. Woest, I. Hearn, S. Lennon, Investigation into the corrosion behaviour of galvanized finned tubing for cooling under deluge enhanced wet/dry cooling conditions, ESCOM, Scientific Investigations Report, 1991.

[15] C. Kutscher, D. Costenaro, Assessment of Evaporative Cooling Enhancement Methods for Air-Cooled Geothermal Power Plants: Preprint, in: Research Org.: National Renewable Energy Lab., Golden, CO. (US), 2002. https://www.osti.gov/servlets/purl/15000953.

[16] H. Reuter, N. Anderson, Performance evaluation of a bare tube air-cooled heat exchanger bundle in wet and dry mode, Appl. Therm. Eng. 105 (2016) 1030–1040. doi:10.1016/j.applthermaleng.2016.06.008.

[17] Z. Li, X. Xu, K. Li, Y. Chen, G. Huang, C. Chen, C.-H. Chen, A flapping vortex generator for heat transfer enhancement in a rectangular airside fin, Int. J. Heat Mass Transf. 118 (2018) 1340–1356. doi:10.1016/j.ijheatmasstransfer.2017.11.067.
[18] S.P. Benn, L.M. Poplaski, A. Faghri, T.L. Bergman, Analysis of thermosyphon/heat pipe integration for feasibility of dry cooling for thermoelectric power generation, Appl. Therm. Eng. 104 (2016) 358–374. doi:10.1016/j.applthermaleng.2016.05.045.
[19] K. Yousef, A. Assefa, A. Hegazy, A. Engeda, Comparative Study of Using R-410A, R-407C, R-22, and R-134a as Cooling Medium in the Condenser of a Steam Power Plant, J. Eng. Gas Turbines Power. 137 (2014) 22002-22002–9. doi:10.1115/1.4028266.
[20] S.G. Kandlikar, A.V. Bapat, Evaluation of Jet Impingement, Spray and Microchannel Chip Cooling Options for High Heat Flux Removal, Heat Transf. Eng. 28 (2007) 911–923. doi:10.1080/01457630701421703.
[21] D.-Y. Lee, K. Vafai, Comparative analysis of jet impingement and microchannel cooling for high heat flux applications, Int. J. Heat Mass Transf. 42 (1999) 1555–1568. doi:10.1016/S0017-9310(98)00265-8.
[22] S. Polat, Heat and mass transfer in impingement drying, Dry. Technol. 11 (1993) 1147–1176.
[23] S. Narayanan, A.G. Fedorov, Y.K. Joshi, Heat and mass transfer during evaporation of thin liquid films confined by nanoporous membranes subjected to air jet impingement, Int. J. Heat Mass Transf. 58 (2013) 300–311.
[24] W.K. Lewis, W.G. Whitman, Principles of Gas Absorption., Ind. Eng. Chem. 16 (1924) 1215–1220. doi:10.1021/ie50180a002.
[25] E. Eckert, Analogies to heat transfer processes Measurements in Heat Transfer (Edited by ERG Eckert and RJ Goldstein), Hemisphere Wash. DC. (1976) 397–423.
[26] Y. Cengel, Heat Transfer: A Practical Approach, 2nd ed., McGraw-Hill, p.760, n.d.
[27] T.L. Bergman, F.P. Incropera, D.P. DeWitt, A.S. Lavine, Fundamentals of heat and mass transfer, 7th ed., John Wiley & Sons, 937, 2011.
[28] T. Kusuda, Calculation of the temperature of a flat-plate wet surface under adiabatic conditions with respect to the Lewis relation, Humidity Moisture Meas. Control Sci. Ind. (1965) 16.
[29] V.G. Levich, Physicochemical hydrodynamics., Prentice-Hall, Englewood Cliffs, N.J., 1962.
[30] P. Tie, Q. Li, Y. Xuan, Investigation on the submerged liquid jet arrays impingement cooling, Appl. Therm. Eng. 31 (2011) 2757–2763. doi:10.1016/j.applthermaleng.2011.04.048.
[31] N. Molloy, Impinging jet flow in a 2-phase system-basic flow pattern, J. Iron Steel Inst. 208 (1970) 943.
[32] M.A. Ehteram, H.B. Tabrizi, G. Ahmadi, M. Safari, M.A. Mirsalim, Investigation of fine droplet generation from hot engine oil by impinging gas jets onto liquid surface, J. Aerosol Sci. 65 (2013) 49–57.
[33] H.. Hwang, G.A. Irons, A water model study of impinging gas jets on liquid surfaces, Metall. Mater. Trans. B. 43 (2011) 302–315.
[34] M. Ersson, A. Tilliander, L. Jonsson, P. Jönsson, A Mathematical Model of an Impinging Air Jet on a Water Surface, ISIJ Int. 48 (2008) 377–384. doi:10.2355/isijinternational.48.377.

[35] M. Adib, M.A. Ehteram, H. Basirat Tabrizi, Numerical and experimental study of oscillatory behavior of liquid surface agitated by high-speed gas jet, Appl. Math. Model. 62 (2018) 510–525. doi:10.1016/j.apm.2018.05.031.
[36] T.L. Bergman, F.P. Incropera, D.P. DeWitt, A.S. Lavine, Fundamentals of heat and mass transfer, John Wiley & Sons, 1010, 2011.
[37] W.-L. Cheng, W.-W. Zhang, H. Chen, L. Hu, Spray cooling and flash evaporation cooling: the current development and application, Renew. Sustain. Energy Rev. 55 (2016) 614–628.
[38] A. Alsaiari, Diller, Thomas E., Experimental Evaluation of Jet Impingement Cooling For Application in Power Plants Condensers, Am. Soc. Therm. Fluids Eng. (n.d.) 2377–2392. doi:10.1615/TFEC2017.iac.017571.
[39] J.S. Maulbetsch, M.N. DiFilippo, Cost and value of water use at combined cycle power plants, Calif. Energy Comm. (2006).

CONCLUSIONS

Jet impingement cooling experiments were conducted on a flat surface in a manner that imitate a condensation process. The results were used to show that jet impingement is a viable and efficient alternative to A-frame ACC's and wet cooling towers. An efficient heat transfer process results in high exhaust temperatures, which results in a decrease in heat transfer due to entrainment of the exhaust by the jets. This effect was modeled and included in a correlation for jet impingement heat transfer. The correlation yielded good prediction accuracy particularly at conditions where entrainment effects are dominant. The findings of the experiment strongly suggest that jet impingement is an alternative that can provide higher rates of heat transfer at lower fan power requirements. Cooling performance *CP* provides an easy quantification of cost-to-benefit of the system. Much higher *CP* values where demonstrated for jet impingement systems than typical current condensers.

Array jet impingement on a constant temperature surface with rectangular grooves resulted on enhancement of heat transfer in comparison to impingement on flat Surface. This was observed experimentally in this study with results uncertainty of 7%. The increase in surface area due to the grooves ranged from 95% to 194%, depending on the geometry, in comparison to the flat surface. However, heat transfer enhancement due to the grooves only ranged from 15% to 63% when compared to the flat surface results. Higher percentage of enhancement in heat transfer was observed in conditions of high H/d_e ratios, large orifice diameters, and jet velocities. The relative position of the jets to the grooves showed no statistically significant effect on heat transfer. Examination of the effect of grooves width and grooves depth on heat transfer showed the effects to be insignificant.

A new approach of hybrid jet impingement cooling was proposed as an alternative for steam condensers of thermoelectric power plants. Jets cooled a grooved surface at a constant temperature with the grooves containing water. The mass transfer analogy provided accurate predictions for the simultaneous process of heat and mass transfer. High magnitudes of heat flux were observed at low jet speeds and flow rates using hybrid jet impingement cooling. Similar heat transfer behavior to jet impingement on a flat was observed for hybrid jet impingement as q" changes with changing operation conditions. Heat transfer of hybrid jet impingement showed 500% improvement as compare to jet impingement on a flat surface. Hybrid jet impingement showed 600% to 1,500% improvement on the thermal performance as compared to air-cooled condensers and wet cooling towers. The proposed approach allows the efficient use of water since evaporation energy is absorbed from the steam and not used to cool air as in conventional evaporative cooling techniques. Hybrid jet impingement cooling is not constrained by the wet-bulb temperature as it is the case for cooling towers, spray cooling, and mist cooling. The results encourage the application of hybrid jet impingement to the condensers of thermoelectric power plants and other relative fields such as air-conditioning and refrigeration.